10-10 October 2010

TECH BRIEFS

NATIONAL AERONAUTICS AND SPACE ADMINISTRATION

INTRODUCTION

Tech Briefs are short announcements of innovations originating from research and development activities of the National Aeronautics and Space Administration. They emphasize information considered likely to be transferable across industrial, regional, or disciplinary lines and are issued to encourage commercial application.

Availability of NASA Tech Briefs and TSPs

Requests for individual Tech Briefs or for Technical Support Packages (TSPs) announced herein should be addressed to

National Technology Transfer Center

Telephone No. **(800) 678-6882** or via World Wide Web at **www.nttc.edu**

Please reference the control numbers appearing at the end of each Tech Brief. Information on NASA's Innovative Partnerships Program (IPP), its documents, and services is also available at the same facility or on the World Wide Web at **http://www.nasa.gov/offices/ipp/network/index.html**

Innovative Partnerships Offices are located at NASA field centers to provide technology-transfer access to industrial users. Inquiries can be made by contacting NASA field centers listed below.

Ames Research Center
Lisa L. Lockyer
(650) 604-1754
lisa.l.lockyer@nasa.gov

Dryden Flight Research Center
Yvonne D. Gibbs
(661) 276-3720
yvonne.d.gibbs@nasa.gov

Glenn Research Center
Kathy Needham
(216) 433-2802
kathleen.k.needham@nasa.gov

Goddard Space Flight Center
Nona Cheeks
(301) 286-5810
nona.k.cheeks@nasa.gov

Jet Propulsion Laboratory
Andrew Gray
(818) 354-4906
gray@jpl.nasa.gov

Johnson Space Center
information
(281) 483-3809
jsc.techtran@mail.nasa.gov

Kennedy Space Center
David R. Makufka
(321) 867-6227
david.r.makufka@nasa.gov

Langley Research Center
Elizabeth B. Plentovich
(757) 864-2857
elizabeth.b.plentovich@nasa.gov

Marshall Space Flight Center
Jim Dowdy
(256) 544-7604
jim.dowdy@msfc.nasa.gov

Stennis Space Center
Ramona Travis
(228) 688-3832
ramona.e.travis@nasa.gov

Carl Ray, Program Executive
Small Business Innovation Research (SBIR) & Small Business Technology Transfer (STTR) Programs
(202) 358-4652
carl.g.ray@nasa.gov

Doug Comstock, Director
Innovative Partnerships Program Office
(202) 358-2221
doug.comstock@nasa.gov

TECH BRIEFS

NATIONAL AERONAUTICS AND SPACE ADMINISTRATION

Hybrid Architecture Active Wavefront Sensing and Control

Goddard Space Flight Center, Greenbelt, Maryland

A method was developed for performing relatively high-speed wavefront sensing and control to overcome thermal instabilities in a segmented primary mirror telescope [e.g., James Webb Space Telescope (JWST) at L2], by using the onboard fine guidance sensor (FGS) to minimize expense and complexity. This FGS performs centroiding on a bright star to feed the information to the pointing and control system.

The proposed concept is to beam split the image of the guide star (or use a single defocused guide star image) to perform wavefront sensing using phase retrieval techniques. Using the fine guidance sensor star image for guiding and fine phasing eliminates the need for other, more complex ways of achieving very accurate sensing and control that is needed for UV-optical applications.

The phase retrieval occurs nearly constantly, so passive thermal stability over fourteen days is not required. Using the FGS as the sensor, one can feed segment update information to actuators on the primary mirror that can update the primary mirror segment fine phasing with this frequency. Because the thermal time constants of the primary mirror are very slow compared to this duration, the mirror will appear extremely stable during observations (to the level of accuracy of the sensing and control). The sensing can use the same phase retrieval techniques as the JWST by employing an additional beam splitter, and having each channel go through a weak lens (one positive and one negative). The channels can use common or separate detectors. Phase retrieval can be performed onboard. The actuation scheme would include a coarse stage able to achieve initial alignment of several millimeters of range (similar to JWST and can use a JWST heritage sensing approach in the science camera) and a fine stage capable of continual updates.

This work was done by Lee Feinberg, Bruce Dean, and Tupper Hyde of Goddard Space Flight Center. For further information, contact the Goddard Innovative Partnerships Office at (301) 286-5810. GSC-15758-1

Carbon-Nanotube-Based Chemical Gas Sensor

This sensor has applications in leak detectors for the automobile, electronics, and medical industries.

NASA's Jet Propulsion Laboratory, Pasadena, California

Conventional thermal conductivity gauges (e.g. Pirani gauges) lend themselves to applications such as leak detectors, or in gas chromatographs for identifying various gas species. However, these conventional gauges are physically large, operate at high power, and have a slow response time.

A single-walled carbon-nanotube (SWNT)-based chemical sensing gauge relies on differences in thermal conductance of the respective gases surrounding the CNT as it is voltage-biased, as a means for chemical identification. Such a sensor provides benefits of significantly reduced size and compactness, fast response time, low-power operation, and inexpensive manufacturing since it can be batch-fabricated using Si integrated-circuit (IC) process technology.

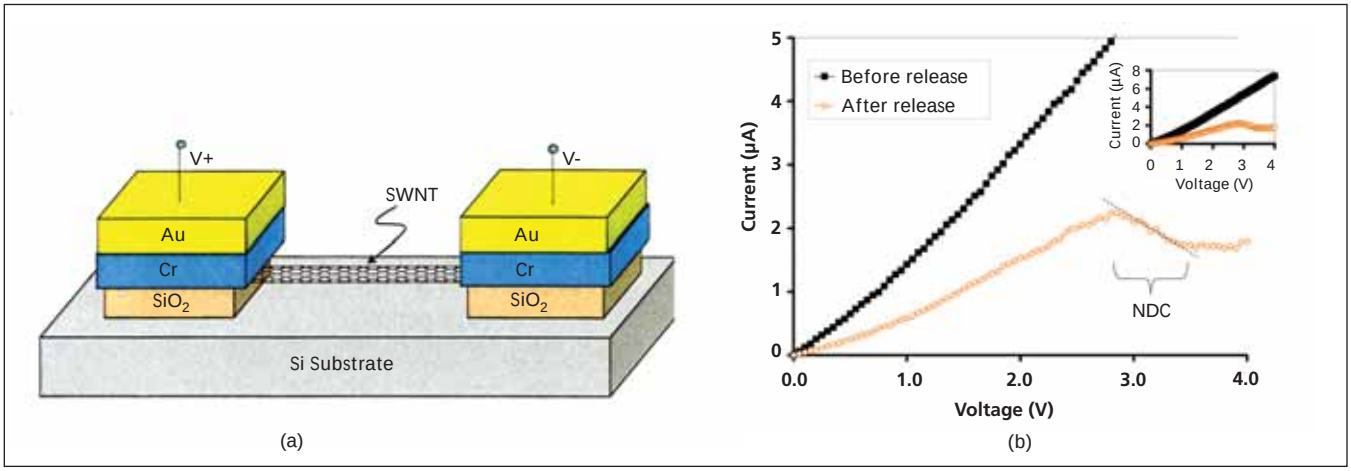

A schematic (a) of the **CNT Gas Pressure or Chemical Sensor**. Au/Cr electrodes anchor the tube during exposure to 10:1 BHF for removing SiO_2 beneath the tubes. Critical point drying in an IPA bath is used for the final release. (b) The comparison of conductance for an unsuspended and suspended tube. The suspended tube shows a negative differential conductance (NDC) regime. The inset shows the current is still linear up to a current as large as 8 μA for the unsuspended tube.

The mechanism by which the sensing occurs is enabled by the reduced dimensionality for phonon scattering in 1D systems — in particular, suspended SWNTs — which can cause unique effects to arise at large bias voltages and power. Such effects are completely absent in 2D or 3D conductors such as within the filament of a conventional Pirani gauge. In suspended SWNTs at high fields, a large non-equilibrium optical phonon population exists, and their long relaxation times result in non-isothermal conditions along the length of the tube. In unsuspended tubes, the I-V characteristic increases monotonically at high voltages suggestive of isothermal conditions, since the substrate facilitates in the relaxation of optical phonons emitted through electron scattering. In contrast, the current in the suspended tube saturates and a negative differential conductance (NDC) regime is encountered, which cannot be explained by velocity saturation (at –5 kV/cm). This is a signature of the effective temperature rise within the tube that can be used to enhance sensitivity for gas detection. The large optical phonon density in suspended SWNTs at high fields with long lifetimes may play an important role in determining the rate of temperature rise in the tubes, which can be exploited maximally for their utility as thermal conductivity-based gas sensors.

The method used to form suspended long (>5 μm) SWNTs is novel and has not been reported in the past. A dry release technique is used based on critical-point drying. In the past, the reduced surface tension of various solvents has been used; however, these are all based on wet processes that will inherently suffer to a larger extent from capillary forces upon release.

The SWNT-based chemical sensor described here could be useful for future NASA astrobiology missions to detect specific biomarkers in the gaseous phase or to decipher biological activity by measuring outgassing rates; for example, within microcavities. The sensor could be used in future NASA instruments that require gas chromatographs to identify chemical species in planetary atmospheres, as well as future Lander missions.

The sensor could also be used aboard NASA spacecraft or instruments as a low-power, low-mass, compact leak detector with a fast response time compared to conventionally used thermal-conductivity-based leak detectors such as the Pirani gauge.

This work was done by Anupama B. Kaul of Caltech for NASA's Jet Propulsion Laboratory. For more information, contact iaoffice@jpl.nasa.gov.

In accordance with Public Law 96-517, the contractor has elected to retain title to this invention. Inquiries concerning rights for its commercial use should be addressed to:

Innovative Technology Assets Management
JPL
Mail Stop 202-233
4800 Oak Grove Drive
Pasadena, CA 91109-8099
E-mail: iaoffice@jpl.nasa.gov

Refer to NPO-46844, volume and number of this NASA Tech Briefs *issue, and the page number.*

Aerogel-Positronium Technology for the Detection of Small Quantities of Organic and/or Toxic Materials

Potential applications range from life detection and human life support, to sample return missions.

NASA's Jet Propulsion Laboratory, Pasadena, California

The Ps-aerogel system [Ps is positronium (an electron-positron-hydrogen-like atom)] has been evaluated and optimized as a potential tool for planetary exploration missions. Different configurations of use were assessed, and the results provide a quantitative measure of the expected performance. The aerogel density is first optimized to attain maximum production of Ps that reaches the pores of the aerogel. This has been accomplished, and the optimum aerogel density is ≈70 mg/cm^3. The aerogel is used as a concentrator for target volatile moieties, which accumulate in its open porosity over an extended period of time. For the detection of the accumulated materials, the use of Ps as a probe for the environment at the pore surface, has been proposed.

This concept is based on two steps: (1) using aerogel to produce Ps and (2) using the propensity of Ps to interact differently with organic and inorganic matter. The active area of such a detector will comprise aerogel with a certain density, specific surface area, and gas permeability optimized for Ps production and gas diffusion and adsorption. The aerogel is a natural adsorber of organic molecules, which adhere to its internal surface, where their presence is detected by the Ps probe. Initial estimates indicate that, e.g., trace organic molecules in the Martian atmosphere, can be detected at the ppm level, which rivals current methods having significantly higher complexity, volume, mass, and power consumption (e.g. Raman, IR).

This method carries important benefits in working toward NASA/JPL goals, and has the potential to advance organic detection capabilities. It is intended to work toward feasibility studies. At the same time, it is recognized that a full-scale investigation will profit enormously from an achieved optimization of the aerogel microstructure for Ps production and gas percolation.

The Ps-aerogel system provides an entirely new approach toward sensing of trace volatile components in vacuum or in the atmosphere. Contrary to all other conventional methods, which use "momentary sensing" and analyzing the content, the Ps-aerogel system relies on a continuous passive exposure to the environment. An instrument built on this new technology will be lightweight, small in size, and will not consume power during accumulation. In testing, the adsorption of simple organic materials, such as alcohols, naphthalene, etc, has been detected. Also, with the optimization of the Ps-aerogel system, a number of other applications, ranging from thermal insulation to charge storage systems, have been discovered.

This work was done by Mihail P. Petkov and Steven M. Jones of Caltech for NASA's Jet Propulsion Laboratory. Further information is contained in a TSP (see page 1). ***NPO-46762***

Graphene-Based Reversible Nano-Switch/Sensor Schottky Diode

This device can extend applications of nanoelectronics to embedded bio-medical devices and explosive-detection devices.

John H. Glenn Research Center, Cleveland, Ohio

This proof-of-concept device consists of a thin film of graphene deposited on an electrodized doped silicon wafer. The graphene film acts as a conductive path between a gold electrode deposited on top of a silicon dioxide layer and the reversible side of the silicon wafer, so as to form a Schottky diode. By virtue of the two-dimensional nature of graphene, this device has extreme sensitivity to different gaseous species, thereby serving as a building block for a volatile species sensor, with the attribute of having reversibility properties. That is, the sensor cycles between active and passive sensing states in response to the presence or absence of the gaseous species.

In addition, because of the sensitivity and diode properties, the device can be used as a switch where its operational stages (i.e., open/closed, on/off) could be controlled by a given gaseous species. Consequently, this proof-of-concept has great potential as a building block for implementation of a switch/sensor device for harsh, embedded, or enclosed environments (e.g., the human body, space-based habitats, airplanes, subways, etc.) where the longevity and reusability of the circuit are critical for reliable operation.

The sensing performance of this device has been experimentally tested in an ambient atmosphere, as well as under an ammonia gas (NH_3) atmosphere. The experimental data demonstrate the dual switching/sensing nature of the nano Schottky diode, hence, the acronym nanoSSSD. Accordingly, the reversible behavior makes the diode suitable for nano-sensing devices intended for applications where access to the sensor, and its potential replacement opportunities, are limited.

The graphene-based nanoSSSD consists of an n-doped or p-doped silicon substrate with a 200-nm thermally grown layer of silicon dioxide (SiO_2). The responsiveness of the diode will depend on the substrate doping type. The oxide layer is in turn electrodized with metallic conductors (e.g., gold) upon which a nanolayer of graphene is deposited so as to wrap around the edge of the electrode to establish a conductive path with the silicon substrate, thereby forming the Schottky diode. The performance of the diode is activated by applying DC voltage between the top metal electrode and the silicon substrate.

Upon exposing the nanoSSSD to a volatile species environment, the diode response is unambiguously different from that manifested under normal ambient conditions. More relevant yet, the behavior is reversible with the performance of the diode returning to its normal operational mode as the volatile species is removed. This feature forms the basis for the functional operation of the device resulting in a reliable, long MTBF (mean time between failure) nano-switch/sensor, ideal for applications where frequent replacement of the device is not a viable option.

This work was done by Félix A. Miranda, Michael A. Meador, and Onoufrios Theofylaktos of Glenn Research Center; Nicholas J. Pinto of the University of Puerto Rico; Carl H. Mueller of Qinetiq North America (Analex Corporation); and Javier Santos-Pérez of Ohio Aerospace Institute. Further information is contained in a TSP (see page 1).

Inquiries concerning rights for the commercial use of this invention should be addressed to NASA Glenn Research Center, Innovative Partnerships Office, Attn: Steve Fedor, Mail Stop 4–8, 21000 Brookpark Road, Cleveland, Ohio 44135.
Refer to LEW-18477-1.

Inductive Non-Contact Position Sensor

John F. Kennedy Space Center, Florida

Optical hardware has been developed to measure the depth of defects in the Space Shuttle Orbiter's windows. In this hardware, a mirror is translated such that its position corresponds to the defect's depth, so the depth measurement problem is transferred to a mirror-position measurement problem. This is preferable because the mirror is internal to the optical system and thus accessible. Based on requirements supplied by the window inspectors, the depth of the defects needs to be measured over a range of 200 microns with a resolution of about 100 nm and an accuracy of about 400 nm. These same requirements then apply to measuring the position of the mirror, and in addition, since this is a scanning system, a response time of about 10 ms is needed.

A market search was conducted and no sensor that met these requirements that also fit into the available housing volume (less than one cubic inch) was found, so a novel sensor configuration was constructed to meet the requirements. This new sensor generates a nearly linearly varying magnetic field over a small region of space, which can easily be sampled, resulting in a voltage proportional to position.

Experiments were done with a range of inductor values, drive voltages, drive frequencies, and inductor shapes. A rough mathematical model was developed for the device that, in most aspects, describes how it operates and what electrical parameters should be chosen for best performance. The final configuration met all the requirements, yielding a small rugged sensor that was easy to use and had nanometer-resolution over more than the 200-μm range required.

The inductive position sensor is a compact device (potentially as small as 2 cm^3), which offers nanometer-position resolution over a demonstrated range of nearly 1 mm. One of its advantages is the simplicity of its electri-

cal design. Also, the sensor resolution is nearly uniform across its operational range, which is in contrast to eddy current and capacitive sensors whose sensitivity is dependent upon position.

This work was done by Robert Youngquist and Alyssa Garcia of Kennedy Space Center and Stephen Simmons of ASRC Aerospace Corporation. For additional information, contact the Kennedy Innovative Partnerships Program Office at 321-867-5033. KSC-13265

High-Temperature Surface-Acoustic-Wave Transducer

This thin, high-temperature-resistant sensor is designed for crack inspections.

John H. Glenn Research Center, Cleveland, Ohio

Aircraft-engine rotating equipment usually operates at high temperature and stress. Non-invasive inspection of microcracks in those components poses a challenge for the non-destructive evaluation community. A low-profile ultrasonic guided wave sensor can detect cracks *in situ*. The key feature of the sensor is that it should withstand high temperatures and excite strong surface wave energy to inspect surface/subsurface cracks. As far as the innovators know at the time of this reporting, there is no existing sensor that is mounted to the rotor disks for crack inspection; the most often used technology includes fluorescent penetrant inspection or eddy-current probes for disassembled part inspection.

An efficient, high-temperature, low-profile surface acoustic wave transducer design has been identified and tested for nondestructive evaluation of structures or materials. The development is a Sol-Gel bismuth titanate-based surface-acoustic-wave (SAW) sensor that can generate efficient surface acoustic waves for crack inspection. The produced sensor is very thin (submillimeter), and can generate surface waves up to 540 °C. Finite element analysis of the SAW transducer design was performed to predict the sensor behavior, and experimental studies confirmed the results.

One major uniqueness of the Sol-Gel bismuth titanate SAW sensor is that it is easy to implement to structures of various shapes. With a spray coating process, the sensor can be applied to surfaces of large curvatures. Second, the sensor is very thin (as a coating) and has very minimal effect on airflow or rotating equipment imbalance. Third, it can withstand temperatures up to 530 °C, which is very useful for engine applications where high temperature is an issue.

This work was done by Xiaoliang Zhao of Intelligent Automation, Inc. and Bernhard R. Tittmann of Pennsylvania State University for Glenn Research Center. Further information is contained in a TSP (see page 1).

Inquiries concerning rights for the commercial use of this invention should be addressed to NASA Glenn Research Center, Innovative Partnerships Office, Attn: Steven Fedor, Mail Stop 4–8, 21000 Brookpark Road, Cleveland, Ohio 44135. Refer to LEW-18547-1.

Grid-Sphere Electrodes for Contact With Ionospheric Plasma

Marshall Space Flight Center, Alabama

Grid-sphere electrodes have been proposed for use on the positively biased end of electrodynamic space tethers. A grid-sphere electrode is fabricated by embedding a wire mesh in a thin film from which a spherical balloon is formed. The grid-sphere electrode would be deployed from compact stowage by inflating the balloon in space. The thin-film material used to inflate the balloon is formulated to vaporize when exposed to the space environment. This would leave the bare metallic spherical grid electrode attached to the tether, which would present a small cross-sectional area (essentially, the geometric wire shadow area only) to incident neutral atoms and molecules. Most of the neutral particles, which produce dynamic drag when they impact a surface, would pass unimpeded through the open grid spaces. However, partly as a result of buildup of a space charge inside the grid-sphere, and partially, the result of magnetic-field effects, the electrode would act almost like a solid surface with respect to the flux of electrons. The net result would be that grid-sphere electrodes would introduce minimal aerodynamic drag, yet have effective electrical-contact surface areas large enough to collect multiampere currents from the ionospheric plasma that are needed for operation of electrodynamic tethers. The vaporizable-balloon concept could also be applied to the deployment of large radio antennas in outer space.

This work was done by Nobie H. Stone and Garrett D. Poe of SRS Technologies for Marshall Space Flight Center. For further information, contact Sammy Nabors, MSFC Commercialization Assistance Lead, at sammy.a.nabors@nasa.gov. Refer to MFS-32567-1.

Enabling IP Header Compression in COTS Routers via Frame Relay on a Simplex Link

This algorithm allows commercial off-the-shelf routers to enter IP header compression mode without the need for a bidirectional handshake.

NASA's Jet Propulsion Laboratory, Pasadena, California

NASA is moving toward a network-centric communications architecture and, in particular, is building toward use of Internet Protocol (IP) in space. The use of IP is motivated by its ubiquitous application in many communications networks and in available commercial off-the-shelf (COTS) technology. The Constellation Program intends to fit two or more voice (over IP) channels on both the forward link to, and the return link from, the Orion Crew Exploration Vehicle (CEV) during all mission phases. Efficient bandwidth utilization of the links is key for voice applications.

In Voice over IP (VoIP), the IP packets are limited to small sizes to keep voice latency at a minimum. The common voice codec used in VoIP is G.729. This new algorithm produces voice audio at 8 kbps and in packets of 10-milliseconds duration.

Constellation has designed the VoIP communications stack to use the combination of IP/UDP/RTP protocols where IP carries a 20-byte header, UDP (User Datagram Protocol) carries an 8-byte header, and RTP (Real Time Transport Protocol) carries a 12-byte header. The protocol headers total 40 bytes and are equal in length to a 40-byte G.729 payload, doubling the VoIP latency. Since much of the IP/UDP/RTP header information does not change from IP packet to IP packet, IP/UDP/RTP header compression can avoid transmission of much redundant data as well as reduce VoIP latency. The benefits of IP header compression are more pronounced at low data rate links such as the forward and return links during CEV launch.

IP/UDP/RTP header compression codecs are well supported by many COTS routers. A common interface to the COTS routers is through frame relay. However, enabling IP header compression over frame relay, according to industry standard (Frame Relay IP Header Compression Agreement FRF.20), requires a duplex link and negotiations between the compressor router and the decompressor router. In Constellation, each forward to and return link from the CEV in space is treated independently as a simplex link. Without negotiation, the COTS routers are prevented from entering into the IP header compression mode, and no IP header compression would be performed.

An algorithm is proposed to enable IP header compression in COTS routers on a simplex link with no negotiation or with a one-way messaging. In doing so, COTS routers can enter IP header compression mode without the need to handshake through a bidirectional link as required by FRF.20. This technique would spoof the routers locally and thereby allow the routers to enter into IP header compression mode without having the negotiations between routers actually occur. The spoofing function is conducted by a frame relay adapter (also COTS) with the capability to generate control messages according to the FRF.20 descriptions. Therefore, "negotiation" is actually performed between the FRF.20 adapter and the connecting COTS router locally and never occurs over the space link. Through understanding of the handshaking protocol described by FRF.20,

the necessary FRF.20 negotiations messages can be generated to control the connecting router, not only to turn on IP header compression but also to adjust the compression parameters. The FRF.20 negotiation (or control) message is composed in the FRF.20 adapter by interpreting the incoming router request message. Many of the fields are simply transcribed from request to response while the control field indicating response and type are modified.

This work was done by Sam P. Nguyen, Jackson Pang, Loren P. Clare, and Michael K. Cheng of Caltech for NASA's Jet Propulsion Laboratory. Further information is contained in a TSP (see page 1). **NPO-47052**

Ka-Band SiGe Receiver Front-End MMIC for Transponder Applications

New architecture improves the quality of the down-converted IF quadrature signals.

NASA's Jet Propulsion Laboratory, Pasadena, California

A fully integrated, front-end Ka-band monolithic microwave integrated circuit (MMIC) was developed that houses an LNA (low noise amplifier) stage, a down-conversion stage, and output buffer amplifiers. The MMIC design employs a two-step quadrature down-conversion architecture, illustrated in the figure, which results in improved quality of the down-converted IF quadrature signals. This is due to the improved sensitivity of this architecture to amplitude and phase mismatches in the quadrature down-conversion process. Current sharing results in reduced power consumption, while 3D-coupled inductors reduce the chip area. Improved noise figure is expected over previous SiGe-based, front-end designs.

This is the first SiGe-based receiver front-end that is capable of finding use in multiple transponder instrument programs. The design uses the latest IBM8HP SiGe process, thereby allowing for improved MMIC performance in the mm-wave regime. Improved performance is expected in terms of power consumption, quality of down-converted signals, and receiver noise figure over SiGe-based designs published by the Air Force Research Laboratory (AFRL) and the Army Research Lab (ARL).

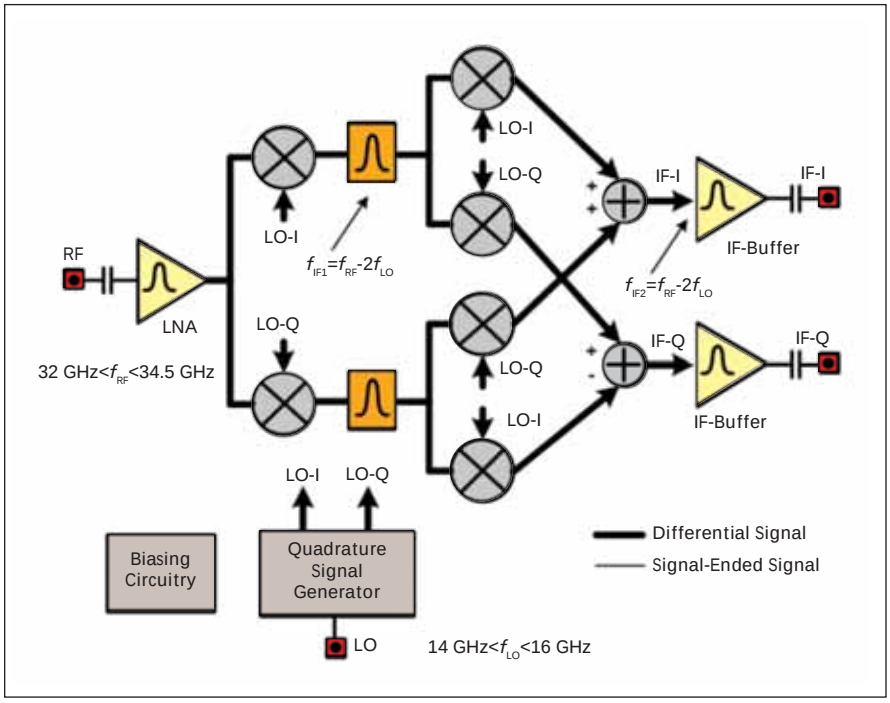

Ka-Band SiGe-Based Receiver front-end MMIC architecture.

This work was done by Jaikrishna Venkatesan and Narayan R. Mysoor of Caltech and Hossein Hashemi and Firooz Aflatouni of the University of Southern California for NASA's Jet Propulsion Laboratory. Further information is contained in a TSP (see page 1). **NPO-42708**

Robust Optimization Design Algorithm for High-Frequency TWTs

A TWT amplifier design algorithm has applications in remote sensing, biomedical imaging, and detection of explosives and toxic biochemical agents.

John H. Glenn Research Center, Cleveland, Ohio

Traveling-wave tubes (TWTs), such as the Ka-band (26-GHz) model recently developed for the Lunar Reconnaissance Orbiter, are essential as communication amplifiers in spacecraft for virtually all near- and deep-space missions. This innovation is a computational design algorithm that, for the first time, optimizes the efficiency and output power of a TWT while taking into account the effects of dimensional tolerance variations.

Because they are primary power consumers and power generation is very expensive in space, much effort has been exerted over the last 30 years to increase the power efficiency of TWTs. However, at frequencies higher than about 60

GHz, efficiencies of TWTs are still quite low. A major reason is that at higher frequencies, dimensional tolerance variations from conventional micromachining techniques become relatively large with respect to the circuit dimensions. When this is the case, conventional design-optimization procedures, which ignore dimensional variations, provide inaccurate designs for which the actual amplifier performance substantially underperforms that of the design. Thus, this new, robust TWT optimization design algorithm was created to take account of and ameliorate the deleterious effects of dimensional variations and to increase efficiency, power, and yield of high-frequency TWTs.

This design algorithm can help extend the use of TWTs into the terahertz frequency regime of 300–3000 GHz. Currently, these frequencies are underutilized because of the lack of efficient amplifiers, thus this regime is known as the "terahertz gap." The development of an efficient terahertz TWT amplifier could enable breakthrough applications in space science molecular spectroscopy, remote sensing, nondestructive testing, high-resolution "through-the-wall" imaging, biomedical imaging, and detection of explosives and toxic biochemical agents.

This work was done by Jeffrey D. Wilson of Glenn Research Center and Christine T. Chevalier of Analex Corp. Further information is contained in a TSP (see page 1).

Inquiries concerning rights for the commercial use of this invention should be addressed to NASA Glenn Research Center, Innovative Partnerships Office, Attn: Steve Fedor, Mail Stop 4–8, 21000 Brookpark Road, Cleveland, Ohio 44135. Refer to LEW-18378-1.

Optimal and Local Connectivity Between Neuron and Synapse Array in the Quantum Dot/Silicon Brain

This bio-inspired technique can enable artificial intelligence in computing technology.

NASA's Jet Propulsion Laboratory, Pasadena, California

This innovation is used to connect between synapse and neuron arrays using nanowire in quantum dot and metal in CMOS (complementary metal oxide semiconductor) technology to enable the density of a brainlike connection in hardware. The hardware implementation combines three technologies:

1. Quantum dot and nanowire-based compact synaptic cell (50×50 nm^2) with inherently low parasitic capacitance (hence, low dynamic power $\approx 10^{-11}$ watts/synapse),
2. Neuron and learning circuits implemented in 50-nm CMOS technology, to be integrated with quantum dot and nanowire synapse, and
3. 3D stacking approach to achieve the overall numbers of high density $O(10^{12})$ synapses and $O(10^{8})$ neurons in the overall system.

In a 1-cm^2 of quantum dot layer sitting on a 50-nm CMOS layer, innovators were able to pack a 10^6-neuron and 10^{10}-synapse array; however, the constraint for the connection scheme is that each neuron will receive a non-identical 10^4-synapse set, including itself, via its efficacy of the connection.

This is not a fully connected system where the 100×100 synapse array only has a 100-input data bus and 100-output data bus. Due to the data bus sharing, it poses a great challenge to have a complete connected system, and its constraint within the quantum dot and silicon wafer layer.

For an effective connection scheme, there are three conditions to be met:

1. Local connection.
2. The nanowire should be connected locally, not globally from which it helps to maximize the data flow by sharing the same wire space location.
3. Each synapse can have an alternate summation line if needed (this option is doable based on the simple mask creation).

The $10^3 \times 10^3$-neuron array was partitioned into a 10-block, $10^2 \times 10^3$-neuron array. This building block can be completely mapped within itself (10,000 synapses to a neuron).

This work was done by Tuan A. Duong, Christopher Assad, and Anilkumar P. Thakoor of Caltech for NASA's Jet Propulsion Laboratory. Further information is contained in a TSP (see page 1). NPO-46222

Method and Circuit for *In-Situ* Health Monitoring of Solar Cells in Space

This method has application in solar arrays for powering unmanned vehicles.

John H. Glenn Research Center, Cleveland, Ohio

This innovation represents a method and circuit realization of a system designed to make *in-situ* measurements of test solar-cell operational parameters on orbit using readily available high-temperature and high-ionizing-radiation-tolerant electronic components. This innovation enables on-orbit *in-situ* solar-array health monitoring and is in response to a need recognized by the U.S. Air Force for future solar arrays for unmanned spacecraft. This system can also be constructed out of commercial-grade electronics and can be embedded into terrestrial solar power system as a diagnostics instrument.

This innovation represents a novel approach to I-V curve measurement that is radiation and temperature hard, consumes very few system resources, is economical, and utilizes commercially available components. The circuit will also operate at temperatures as low as –55 °C and up to +225 °C, allowing it to reside close to the array in direct sunlight. It uses a swept mode transistor functioning as a resistive load while utilizing the solar cells

themselves as the biasing device, so the size of the instrument is small and there is no danger of over-driving the cells. Further, this innovation utilizes nearly universal spacecraft bus resources and therefore can be readily adapted to any spacecraft bus allowing for ease of retrofit, or designed into new systems without requiring the addition of infrastructure.

One unique characteristic of this innovation is that it effects the measurement of I-V curves without the use of large resistor arrays or active current sources normally used to characterize cells. A single transistor is used as a variable resistive load across the cell. This multi-measurement instrument was constructed using operational amplifiers, analog switches, voltage regulators, MOSFETs, resistors, and capacitors. The operational amplifiers, analog switches, and voltage regulators are silicon-on-insulator (SOI) technology known for its hardness to the effects of ionizing radiation. The SOI components used can tolerate temperatures up to 225 °C, which gives plenty of thermal headroom allowing this circuit to perhaps reside in the solar cell panel itself where temperatures can reach over 100 °C.

This work was done by Michael J. Krasowski and Norman F. Prokop of Glenn Research Center.

Inquiries concerning rights for the commercial use of this invention should be addressed to NASA Glenn Research Center, Innovative Partnerships Office, Attn: Steve Fedor, Mail Stop 4–8, 21000 Brookpark Road, Cleveland, Ohio 44135. Refer to LEW-18461-1.

Software

BGen: A UML Behavior Network Generator Tool

BGen software was designed for autogeneration of code based on a graphical representation of a behavior network used for controlling automatic vehicles. A common format used for describing a behavior network, such as that used in the JPL-developed behavior-based control system, CARACaS ["Control Architecture for Robotic Agent Command and Sensing" (NPO-43635), *NASA Tech Briefs*, Vol. 32, No. 10 (October 2008), page 40] includes a graph with sensory inputs flowing through the behaviors in order to generate the signals for the actuators that drive and steer the vehicle.

A computer program to translate Unified Modeling Language (UML) Freeform Implementation Diagrams into a legacy C implementation of Behavior Network has been developed in order to simplify the development of C-code for behavior-based control systems. UML is a popular standard developed by the Object Management Group (OMG) to model software architectures graphically. The C implementation of a Behavior Network is functioning as a decision tree.

This work was done by Leonard J. Reder, Terrance L. Huntsberger, and Harry Balian of Caltech for NASA's Jet Propulsion Laboratory. Further information is contained in a TSP (see page 1).

This software is available for commercial licensing. Please contact Daniel Broderick of the California Institute of Technology at danielb@caltech.edu. Refer to NPO-46787.

Platform for Post-Processing Waveform-Based NDE

Signal- and image-processing methods are commonly needed to extract information from the waves, improve resolution of, and highlight defects in an image. Since some similarity exists for all waveform-based nondestructive evaluation (NDE) methods, it would seem that a common software platform containing multiple signal- and image-processing techniques to process the waveforms and images makes sense where multiple techniques, scientists, engineers, and organizations are involved.

NDE Wave & Image Processor Version 2.0 software provides a single, integrated signal- and image-processing and analysis environment for total NDE data processing and analysis. It brings some of the most useful algorithms developed for NDE over the past 20 years into a commercial-grade product. The software can import signal/spectroscopic data, image data, and image series data.

This software offers the user hundreds of basic and advanced signal- and image-processing capabilities including esoteric 1D and 2D wavelet-based de-noising, de-trending, and filtering. Batch processing is included for signal- and image-processing capability so that an optimized sequence of processing operations can be applied to entire folders of signals, spectra, and images. Additionally, an extensive interactive model-based curve-fitting facility has been included to allow fitting of spectroscopy data such as from Raman spectroscopy. An extensive joint-time frequency module is included for analysis of non-stationary or transient data such as that from acoustic emission, vibration, or earthquake data.

This work was done by Don J. Roth of Glenn Research Center. Further information is contained in a TSP (see page 1). Inquiries concerning rights for the commercial use of this invention should be addressed to NASA Glenn Research Center, Innovative Partnerships Office, Attn: Steve Fedor, Mail Stop 4–8, 21000 Brookpark Road, Cleveland, Ohio 44135. Refer to LEW-18460-1.

Electrochemical Hydrogen Peroxide Generator

Stable electrocatalysts can produce hydrogen peroxide under acidic conditions.

Lyndon B. Johnson Space Center, Houston, Texas

Two-electron reduction of oxygen to produce hydrogen peroxide is a much researched topic. Most of the work has been done in the production of hydrogen peroxide in basic media, in order to address the needs of the pulp and paper industry. However, peroxides under alkaline conditions show poor stabilities and are not useful in disinfection applications. There is a need to design electrocatalysts that are stable and provide good current and energy efficiencies to produce hydrogen peroxide under acidic conditions.

The innovation focuses on the *in situ* generation of hydrogen peroxide using an electrochemical cell having a gas diffusion electrode as the cathode (electrode connected to the negative pole of the power supply) and a platinized titanium anode. The cathode and anode compartments are separated by a readily available cation-exchange membrane (Nafion® 117). The anode compartment is fed with deionized water. Generation of oxygen is the anode reaction.

Protons from the anode compartment are transferred across the cation-exchange membrane to the cathode compartment by electrostatic attraction towards the negatively charged electrode. The cathode compartment is fed with oxygen. Here, hydrogen peroxide is generated by the reduction of oxygen. Water may also be generated in the cathode. A small amount of water is also transported across the membrane along with hydrated protons transported across the membrane. Generally, each proton is hydrated with 3–5 molecules.

The process is unique because hydrogen peroxide is formed as a high-purity aqueous solution. Since there are no hazardous chemicals or liquids used in the process, the disinfection product can be applied directly to water, before entering a water filtration unit to disinfect the incoming water and to prevent the build up of heterotrophic bacteria, for example, in carbon based filters.

The competitive advantages of this process are:

1. No consumable chemicals are needed in the process. The only raw materials needed are water and oxygen or air.
2. The product is pure and can therefore be used in disinfection applications directly or after proper dilution with water.
3. Oxygen generated in the anode compartment is used in the electrochemical reduction process; in addition, external oxygen is used to establish a high flow rate in the cathode compartment to remove the desired product efficiently. Exiting oxygen can be recycled after separation of liquid hydrogen peroxide product, if so desired.
4. The process can be designed for peroxide generation under microgravity conditions.
5. High concentrations of the order of 6–7 wt% can be generated by this method. This method at the time of this reporting is superior to what other researchers have reported.
6. The cell design allows for stacking of cells to increase the hydrogen peroxide production.
7. The catalyst mix containing a diquaternary ammonium compound enabled not only higher concentration of hydrogen peroxide but also higher current efficiency, improved energy efficiency, and catalyst stability.
8. The activity of the catalyst is maintained even after repeated periods of system shutdown.
9. The catalyst system can be extended for fuel-cell cathodes with suitable modifications.

This work was done by Charles L.K. Tennakoon, Waheguru Singh, Kelvin C. Anderson, and Thomas Kinney of Lynntech, Inc. for Johnson Space Center.

In accordance with Public Law 96-517, the contractor has elected to retain title to this invention. Inquiries concerning rights for its commercial use should be addressed to:

Lynntech, Inc.
Technology Transfer Office
1302 East Collins Blvd.
Richardson, Texas 75081
Phone No.: (979) 693-0017
E-mail: requests@lynntech.com

Refer to MSC-23874-1, volume and number of this NASA Tech Briefs *issue, and the page number.*

Fabrication of Single, Vertically Aligned Carbon Nanotubes in 3D Nanoscale Architectures

Potential applications of this process are integrated circuits, nano switches, and biological sensors.

NASA's Jet Propulsion Laboratory, Pasadena, California

Plasma-enhanced chemical vapor deposition (PECVD) and high-throughput manufacturing techniques for integrating single, aligned carbon nanotubes (CNTs) into novel 3D nanoscale architectures have been developed. First, the PECVD growth technique ensures excellent alignment of the tubes, since the tubes align in the direction of the electric field in the plasma as they are growing. Second, the tubes generated with this technique are all metallic, so their chirality is predetermined, which is important for electronic applications. Third, a wafer-scale manufacturing process was developed that is high-throughput and low-cost, and yet enables the integration of just single, aligned tubes with nanoscale 3D architectures with unprecedented placement accuracy and does not rely on e-beam lithography. Such techniques should lend

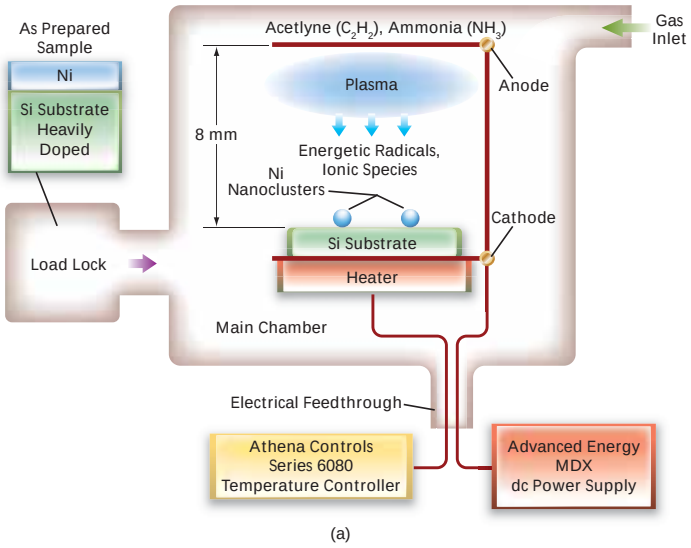

(a)

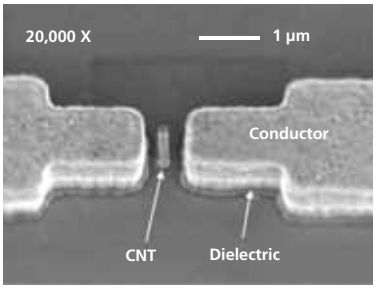

(b)

(a) In the **dc PECVD Growth Chamber**, the sample was placed on a 3-in. (7.6-cm) Mo ring, where the wafer was transported from the load lock to the main chamber. (b) A single, vertically aligned tube is seen centered precisely within deep trenches, which was formed using high throughput processes.

themselves to the integration of PECVD-grown tubes for applications ranging from interconnects, nanoelectromechanical systems (NEMS), sensors, bioprobes, or other 3D electronic devices.

Chemically amplified polyhydroxystyrene-resin-based deep UV resists were used in conjunction with excimer laser-based (λ = 248 nm) step-and-repeat lithography to form Ni catalyst dots ≈300 nm in diameter that nucleated single, vertically aligned tubes with high yield using dc PECVD growth. This is the first time such chemically amplified resists have been used, resulting in the nucleation of single, vertically aligned tubes.

In addition, novel 3D nanoscale architectures have been created using top-down techniques that integrate single, vertically aligned tubes. These were enabled by implementing techniques that use deep-UV chemically amplified resists for small-feature-size resolution; optical lithography units that allow unprecedented control over layer-to-layer registration; and ICP (inductively coupled plasma) etching techniques that result in near-vertical, high-aspect-ratio, 3D nanoscale architectures, in conjunction with the use of materials that are structurally and chemically compatible with the high-temperature synthesis of the PECVD-grown tubes. The techniques offer a wafer-scale process solution for integrating single PECVD-grown nanotubes into novel architectures that should accelerate their integration in 3D electronics in general.

NASA can directly benefit from this technology for its extreme-environment planetary missions. Current Si transistors are inherently more susceptible to high radiation, and do not tolerate extremes in temperature. These novel 3D nanoscale architectures can form the basis for NEMS switches that are inherently less susceptible to radiation or to thermal extremes.

This work was done by Anupama B. Kaul, Krikor G. Megerian, Paul A. Von Allmen, and Richard L. Baron of Caltech for NASA's Jet Propulsion Laboratory. For more information, contact iaoffice@jpl.nasa.gov.

In accordance with Public Law 96-517, the contractor has elected to retain title to this invention. Inquiries concerning rights for its commercial use should be addressed to:

Innovative Technology Assets Management
JPL
Mail Stop 202-233
4800 Oak Grove Drive
Pasadena, CA 91109-8099
E-mail: iaoffice@jpl.nasa.gov

Refer to NPO-46552, volume and number of this NASA Tech Briefs *issue, and the page number.*

Process To Create High-Fidelity Lunar Dust Simulants

Marshall Space Flight Center, Alabama

A method was developed to create high-fidelity lunar dust simulants that better match the unique properties of lunar dust than the existing simulants. The new dust simulant is designed to more closely approximate the size, morphology, composition, and other important properties of lunar dust (including the presence of nanophase iron).

A two-step process is required to create this dust simulant. The first step is to prepare a feedstock material that contains a high percentage of agglutinate-like particles with iron globules (including nanophase iron). The raw material selected must have the proper mineralogical composition. In the second processing step, the feedstock material from the first step is jet-milled to reduce the particle size to a range consistent with lunar dust.

This work was done by Robert Gustafson of Orbital Technologies Corp. for Marshall Space Flight Center. For more information, contact Sammy Nabors, MSFC Commercialization Assistance Lead, at sammy.a.nabors@nasa.gov. Refer to MFS-32729-1.

Lithium-Ion Electrolytes Containing Phosphorous-Based, Flame-Retardant Additives

This technology can enhance the safety of lithium-ion batteries for portable electronic devices and hybrid electric vehicles.

NASA's Jet Propulsion Laboratory, Pasadena, California

Future NASA missions aimed at exploring Mars, the Moon, and the outer planets require rechargeable batteries that can operate over a wide temperature range (–60 to +60 °C) to satisfy the requirements of various applications. In addition, many of these applications will require improved safety, due to their use by humans. Currently, the state-of-the-art lithium-ion (Li-ion) system has been demonstrated to operate over a wide range of temperatures (–40 to +40 °C); however, abuse conditions can often lead to cell rupture and fire. The nature of the electrolyte can greatly affect the propensity of the cell/battery to catch fire, given the flammability of the organic solvents used within.

Li-ion electrolytes have been developed that contain a flame-retardant additive in conjunction with fluorinated co-solvents to provide a safe system with a wide operating temperature range. Previous work incorporated fluorinated esters into multi-component electrolyte formulations, which were demonstrated to cover a temperature range from –60 to +60 °C. This work was described in "Fluoroester Co-Solvents for Low-Temperature Li+ Cells" (NPO-44626), *NASA Tech Briefs*, Vol. 33, No. 9 (September 2009), p. 37; and "Optimized Li-Ion Electrolytes Containing Fluorinated Ester Co-Solvents" (NPO-45824), *NASA Tech Briefs*, Vol. 34, No. 3 (March 2010), p. 48.

Other previous work improved the safety characteristics of the electrolytes by adding flame-retardant additives such as triphenyl phosphate (TPhPh), tributyl phosphate (TBuPh), triethyl phosphate (TEtPh), and bis(2,2,2-trifluoroethyl) methyl phosphonate (TFMPo). The current work involves further investigation of other types of flame-retardant additives, including tris(2,2,2-trifluoroethyl) phosphate, tris(2,2,2-trifluoroethyl) phosphite, triphenylphosphite, diethyl ethylphosphonate, and diethyl phenylphosphonate added to an electrolyte composition intended for wide operating temperatures.

In general, many of the formulations investigated in this study displayed good performance over a wide temperature range, good cycle life characteristics, and are expected to have improved safety characteristics, such as low flammability. Of the electrolytes studied, 1.0 M $LiPF_6$ in EC+EMC+DEP (20:75:5 v/v %) and 1.0 M $LiPF_6$ in EC+EMC+DPP (20:75:5 v/v %) displayed the best operation at low temperatures, whereas the electrolyte containing triphenylphosphite displayed the best cycle life performance compared to the baseline solution. It is anticipated that further improvements can be made to the life characteristics with the incorporation of a SET promoters (such as VC, vinylene carbonate), which will likely inhibit the decomposition of the flame-retardant additives.

This work was done by Marshall C. Smart, Kiah A. Smith, and Ratnakumar V. Bugga of Caltech and G. K. Surya Prakash of the University of Southern California for NASA's Jet Propulsion Laboratory. For more information, contact iaoffice@jpl.nasa.gov.

In accordance with Public Law 96-517, the contractor has elected to retain title to this invention. Inquiries concerning rights for its commercial use should be addressed to:

Innovative Technology Assets Management
JPL
Mail Stop 202-233
4800 Oak Grove Drive
Pasadena, CA 91109-8099
E-mail: iaoffice@jpl.nasa.gov

Refer to NPO-46599, volume and number of this NASA Tech Briefs *issue, and the page number.*

InGaP Heterojunction Barrier Solar Cells

Nanostructured cells could enhance the performance of terrestrial high-efficiency solar cells.

John H. Glenn Research Center, Cleveland, Ohio

A new solar-cell structure utilizes a single, ultra-wide well of either gallium arsenide (GaAs) or indium-gallium-phosphide (InGaP) in the depletion region of a wide bandgap matrix, instead of the usual multiple quantum well layers. These InGaP barrier layers are effective at reducing diode dark current, and photogenerated carrier escape is maximized by the proper design of the electric field and barrier profile. With the new material, open-circuit voltage enhancements of 40 and 100 mV (versus PIN control systems) are possible without any degradation in short-circuit current.

Basic tenets of quantum-well and quantum-dot solar cells are utilized, but instead of using multiple thin layers, a single wide well works better. InGaP is used as a barrier material, which increases open current, while simultaneously lowering dark current, reducing both hole diffusion from the base, and space charge recombination within the depletion region. Both the built-in field and the barrier profile are tailored to enhance thermionic emissions, which maximizes the photocurrent at forward bias, with a demonstrated voltage increase.

An InGaP heterojunction barrier solar cell consists of a single, ultra-wide GaAs, aluminum-gallium-arsenide (AlGaAs), or lower-energy-gap InGaP absorber well placed within the depletion region of an otherwise wide bandgap PIN diode. Photogenerated electron collection is unencumbered in this structure. InGaAs wells can be added to the thick GaAs absorber layer to capture lower-energy photons.

This work was done by Roger E. Welser of Kopin Corporation for Glenn Research Center. Further information is contained in a TSP (see page 1).

Inquiries concerning rights for the commercial use of this invention should be addressed to NASA Glenn Research Center, Innovative Partnerships Office, Attn: Steve Fedor, Mail Stop 4–8, 21000 Brookpark Road, Cleveland, Ohio 44135. Refer to LEW-18393-1

Straight-Pore Microfilter With Efficient Regeneration

John H. Glenn Research Center, Cleveland, Ohio

A novel, high-efficiency gas particulate filter has precise particle size screening, low pressure drop, and a simple and fast regeneration process. The regeneration process, which requires minimal material and energy consumption, can be completely automated, and the filtration performance can be restored within a very short period of time.

This filter media may not be the complete replacement for other filtration technologies, but can be a key component in a complete system. This design removes the majority of airborne particulates, with its fast regeneration time allowing a significant increase in the operating period of other filtration media (if necessary) between replacement/regeneration.

Conventional filter media are based on polymer/glass fibers, but this filter is of a novel material composite that contains the support structure and a novel coating. The support structure gives the filter good mechanical properties, while the novel coating creates a unique regeneration character. Also, this support structure can be prepared by laser micromachining etching (i.e. a chemical laser), or micro-molding technology. A novel coating shell is then formed on the support structure to further reduce the pore diameter.

This work was done by Han Liu, Anthony B. LaConti, Thomas J. McCallum, and Edwin W. Schmitt of Giner Electrochemical Systems, LLC for Glenn Research Center. Further information is contained in a TSP (see page 1).

Inquiries concerning rights for the commercial use of this invention should be addressed to NASA Glenn Research Center, Innovative Partnerships Office, Attn: Steve Fedor, Mail Stop 4–8, 21000 Brookpark Road, Cleveland, Ohio 44135. Refer to LEW-18498-1.

Determining Shear Stress Distribution in a Laminate

The simplified shear solution does not require solution of a particular boundary value problem.

John H. Glenn Research Center, Cleveland, Ohio

A "simplified shear solution" method approximates the through-thickness shear stress distribution within a composite laminate based on an extension of laminated beam theory. The method does not consider the solution of a particular boundary value problem; rather, it requires only knowledge of the global shear loading, geometry, and material properties of the laminate or panel. It is thus analogous to lamination theory in that ply-level stresses can be efficiently determined from global load resultants at a given location in a structure and used to evaluate the margin of safety on a ply-by-ply basis. The simplified shear solution stress distribution is zero at free surfaces, continuous at ply boundaries, and integrates to the applied shear load. The method has been incorporated within the HyperSizer® commercial structural sizing software to improve its predictive capability for designing composite structures.

The HyperSizer structural sizing software is used extensively by NASA to design composite structures. In the case of through-thickness shear loading on panels, HyperSizer previously included a basic, industry-standard, method for approximating the resulting shear stress distribution in sandwich panels. However, no such method was employed for solid laminate panels.

The purpose of the innovation is to provide an approximation of the through-thickness shear stresses in a solid laminate given the through-thickness shear loads (Q_x and Q_y) on the panel. The method was needed for implementation within the HyperSizer structural sizing software so that the approximated ply-level shear stresses could be utilized in a failure theory to assess the adequacy of a panel design.

The simplified shear solution method was developed based on extending and generalizing bi-material beam theory to platelike structures. It is assumed that the through-thickness shear stresses arise due to local bending of the laminate induced by the through-thickness shear load, and by imposing equilibrium both vertically and horizontally, the through-thickness shear stress distribution can be calculated. The resulting shear stresses integrate to the applied shear load, are continuous at the ply interfaces, and are zero at the laminate-free surfaces. If both Q_x and Q_y shear loads are present, it is assumed that they act independently and that their effects can be superposed. The calculated shear stresses can be rotated within each ply to the principal material coordinates for use in a ply-level failure criterion.

The novelty of the simplified shear solution method is its simplicity and the fact that it does not require solution of a particular boundary value problem. The advantages of the innovation are that an approximation of the though-thickness shear stress distribution can be quickly determined for any solid laminate or solid laminate region within a stiffened panel.

This work was done by Brett A. Bednarcyk and Jacob Aboudi of Ohio Aerospace Institute and Phillip W. Yarrington of the Collier Research Corp. for Glenn Research Center. Further information is contained in a TSP (see page 1).

Inquiries concerning rights for the commercial use of this invention should be addressed to NASA Glenn Research Center, Innovative Partnerships Office, Attn: Steve Fedor, Mail Stop 4–8, 21000 Brookpark Road, Cleveland, Ohio 44135. Refer to LEW-18441-1.

Self-Adjusting Liquid Injectors for Combustors

Flow inlet area would vary to maintain optimum pressure drops.

Marshall Space Flight Center, Alabama

A class of self-adjusting injectors for spraying liquid oxidizers and/or fuels into combustion chambers has been proposed. The proposed injectors were originally intended for use in rocket-engine combustion chambers, but could also be used to improve control over flows of liquid propellants in other combustion chambers.

In some applications, there is a need to vary the combustion power. Usually, this requirement is satisfied by throttling either or both propellants injected into a combustion chamber. Most prior injectors work well over small throttling ranges; attempts to use them over wider throttling ranges can result in undesired injection pressure drops that can compromise combustion performance, including giving rise to combustion instability. Some prior injectors have fixed inlet areas. A fixed inlet area is optimum at one flow rate only; if the flow rate is changed, then the pressure drop also changes to a value that, typically, is not optimum. Some other prior injectors have been equipped with externally actuated mechanisms to vary their inlet areas, but, in each case, either the mechanism has been excessively complex or else combustion performance has still been compromised.

The basic idea of the proposed injectors is to use simple mechanisms, inside the injectors themselves, to adjust inlet areas so as to keep injection pressure drops at or near optimum values throughout wide throttling ranges. These mechanisms would be actuated by the very pressure drops that they are intended to regulate.

A typical injector according to the proposal (see figure) would include an injection tube containing multiple inlet slots cut tangentially to the inner surface of the tube. The tangential orientation of these slots would channel the fluid entering the tube through them into a swirling motion. (The tangential orientation of the slots is not an essential element of the proposal; it is mentioned here because swirling injectors are common.) The dimensions and arrange-

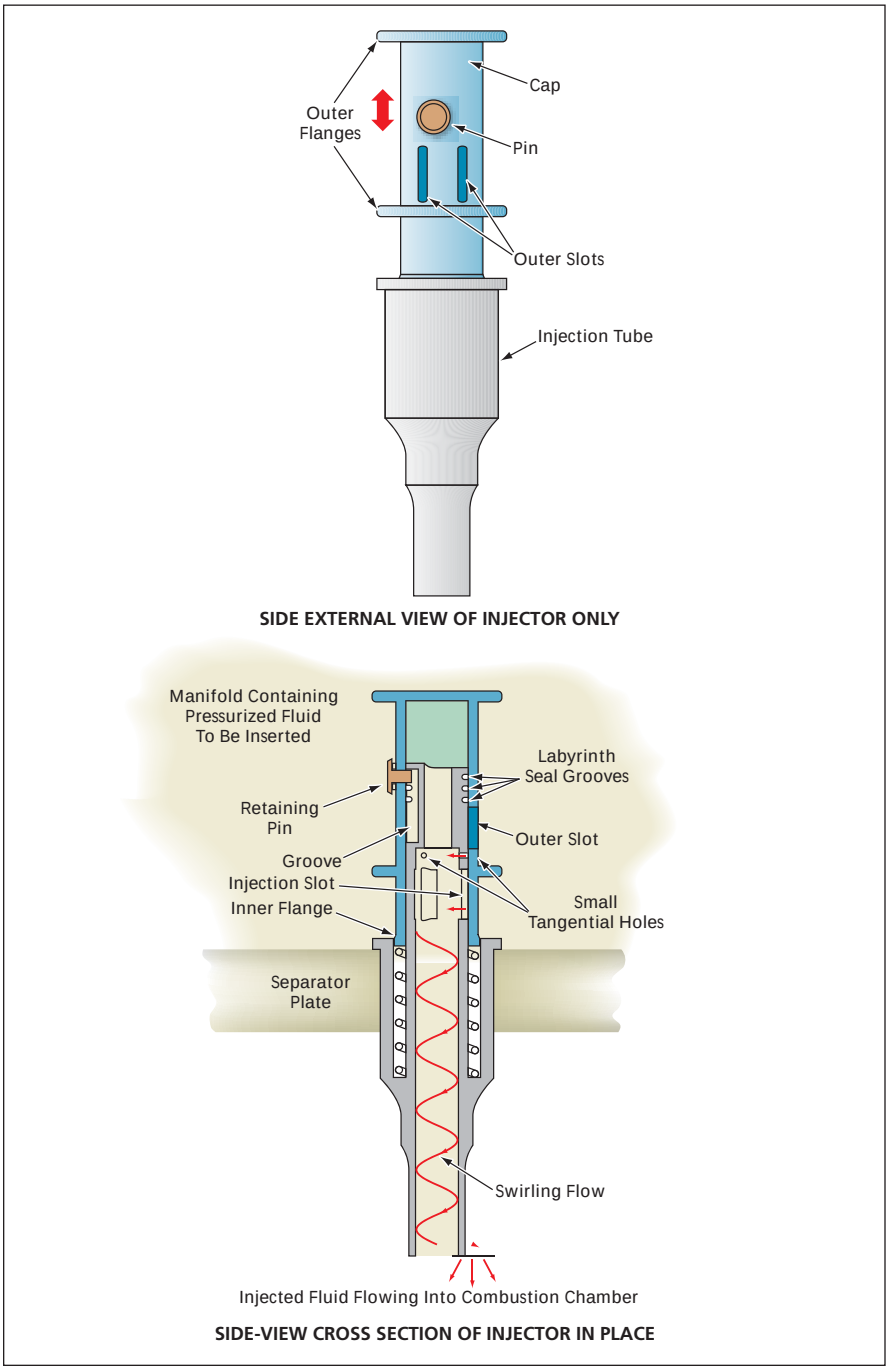

The **Cap Would Slide in the Injector Tube** in response to a change in pressure drop from the manifold above the separator plate to the combustion chamber below the injector outlet. The sliding would expose more or less of the injector-slot area to adjust the pressure drop according to the flow rate. This configuration is representative, not exclusive: the basic self-adjusting-injector concept could be implemented by a variety of mechanisms.

ment of these slots would be chosen, in conjunction with those of other components, to optimize performance.

The upper end of the injection tube would be covered with a cap that would contain a number of outer slots equal to the number of injection slots. The cap would translate axially (up and down in the figure). Two retaining pins (of which one can be seen in the figure) in holes in the cap would protrude into grooves in the injection tube to prevent the cap from coming off the injection tube while allowing the cap to slide freely only within limits. The pins would also keep the outer slots in the cap aligned with the injection slots in the tube.

A coil spring would lie in an annular recess in the injection tube and would be compressed between the bottom of the recess and an inner flange at the bottom of the cap. Small tangential holes could be included, in addition to the outer slots, to allow initial flow at the lowest power level. The cap and the exposed portion of the injector tube would protrude into a manifold containing the fluid to be injected, and outer flanges on the cap would contribute drag between the cap and the fluid to damp any oscillatory motion of the cap, thereby helping to suppress instability. Labyrinth-type seal grooves would prevent gross leakage, so that most of the flow must enter the injection tube either through the tangential slots or the small tangential holes.

In operation, the pressure drop between the manifold and the inside of the cap (which pressure drop would be part of the total pressure drop from the manifold to the combustion chamber) would create a force that would push the cap downward against the spring. This downward motion would cause the outer slots in the cap to partially expose the tangential slots in the injection tube, thereby limiting the pressure drop by increasing the cross-sectional area for flow into the tube. The number and dimensions of the tangential slots would be chosen in conjunction with the stiffness and preload of the spring to obtain the optimum pressure drop as a function of the rate of flow (and, hence, as a function of the combustion power level).

This work was done by Huu Trinh and William Myers of Marshall Space Flight Center.

This invention is owned by NASA, and a patent application has been filed. For further information, contact Sammy Nabors, MSFC Commercialization Assistance Lead, at sammy.a.nabors@nasa.gov. Refer to MFS-32518-1.

Handling Qualities Prediction of an F-16XL-Based Reduced Sonic Boom Aircraft

This technique helps determine how much an aircraft could be modified without affecting its baseline handling qualities.

Dryden Flight Research Center, Edwards, California

A major goal of the Supersonics Project under NASA's Fundamental Aeronautics program is sonic boom reduction of supersonic aircraft. An important part of this effort is development and validation of sonic boom prediction tools used in aircraft design. NASA Dryden's F-16XL was selected as a potential testbed aircraft to provide flight validation.

Part of this task was predicting the handling qualities of the modified aircraft. Due to the high cost of modifying the existing F-16XL control laws, it was desirable to find modifications that reduced the aircraft sonic boom but did not degrade baseline aircraft handling qualities allowing for the potential of flight test without changing the current control laws. This was not a requirement for the initial modification design work, but an important consideration for proceeding to the flight test option.

The primary objective of this work was to determine an aerodynamic and mass properties envelope of the F-16XL aircraft. The designers could use this envelope to determine the effect of proposed modifications on aircraft handling qualities.

The approach to this objective had two parts. First was validation of the existing NASA DFRC F-16XL simulation that would be providing data for this effort, as well as the handling qualities tools that would analyze the data. The second part was modifying the simulation to represent the modified aircraft and determining the modification envelope, which showed how much of the aircraft could be modified without affecting baseline aircraft handling qualities.

Validation of the F-16XL simulation was important as the simulation had not been used for research in over 10 years. Updates and modifications had been made to the simulation for use as a demonstration device. Check case data included with the simulation were compared with data generated from the current simulation and matched almost exactly. Pilot input from flight test data was fed into the simulation, and aircraft response was compared to simulation response.

Validation of the handling qualities tools was also important as these tools had been updated and modified since being used for F-16XL analysis. Flight test and simulation data were input into the handling qualities tools and compared to past results.

With the simulation and handling qualities tools validated, the simulation was modified to represent potential aerodynamic and mass properties changes due to the aircraft modifications. The values of these parameters represent a best guess of how proposed modifications would affect aircraft aerodynamic and mass properties. The parameters selected were those thought to be most affected by the modifications.

The simulator was set up at one of a list of various flight conditions with one of the parameters modified. Pitch and roll frequency sweeps were input into the simulation and simulation response was recorded. These data were then input into the handling qualities tools, and the handling qualities of the modified aircraft were predicted. The final step was to have pilots perform a task in the simulator and make handling qualities ratings and comments. A tracking task was set up in the simulator and performance criteria were defined. This would allow final validation of the handling qualities tools.

This work was done by Bruce Cogan and Seung Yoo of Dryden Flight Research Center. Further information is contained in a TSP (see page 1). **DRC-009-040**

Tele-Robotic ATHLETE Controller for Kinematics —TRACK

TRACK is useful in cases where the whole-limb posture must be unambiguously commanded.

NASA's Jet Propulsion Laboratory, Pasadena, California

TRACK is a specialized controller for the All-Terrain Hex-Limbed Extra-Terrestrial Explorer Robot (ATHLETE), which has six limbs with six kinematic degrees of freedom each. TRACK is a 1/8-scale sensed but un-actuated model of one ATHLETE limb (see figure), designed to be used as a human-interface device to aid operations. TRACK is useful in cases where the whole-limb posture must be unambiguously commanded — for example, to maximize rigidity, available range of motion, or to avoid nearby obstacles. Because TRACK mimics the link lengths and geometry of ATHLETE as well as the joint angle limits, its kinematic workspace is representative of the actual ATHLETE limb workspace.

TRACK includes rotary sensors (potentiometers) for each ATHLETE kinematic degree-of-freedom (DoF) and an extra rotary sensor for the wheel rotation; spring-loaded friction bearings to hold joint pose against gravity; tri-color RGB LEDs (light emitting diodes) at each joint and the wheel; two momentary-contact tactile pushbuttons at each joint and the wheel; USB (universal serial bus) communications and power; onboard firmware with calibration storage and ASCII (American Standard Code for Information Interchange) monitor; and host-side Java interface library.

Tele-Robotic ATHLETE Controller for kinematics.

This work was done by Jeffrey S. Norris of Caltech and Marsette A. Vona of the Massachusetts Institute of Technology for NASA's Jet Propulsion Laboratory. For more information, contact iaoffice@jpl.nasa.gov. NPO-46517

Three-Wheel Brush-Wheel Sampler

New design simplifies sample collection.

NASA's Jet Propulsion Laboratory, Pasadena, California

A new sampler is similar to a common snow blower, but is robust and effective in sample collection. The brush wheels are arranged in a triangle shape, each driven by a brushless DC motor and planetary gearhead embedded in the wheel shaft. Its speed can be varied from 800–2,000 rpm, depending on the surface regolith resistance. The sample-collecting flow path, and internal features, are designed based on flow dynamics, and the sample-collecting rates have consistently exceeded the requirement under various conditions that span the range of expected surface properties.

The brush-wheel sampler (BWS) (as is shown in the figure) is designed so that the flow channel is the main body of the apparatus, and links the brush-wheel assembly to the sample canister. The combination of the three brush wheels, the sample flow path, and the canister location make sample collection, storage, and transfer an easier task.

This work was done by Geoffrey A. Duckworth, Jun Liu, and Mark G. Brown of Caltech for NASA's Jet Propulsion Laboratory. For more information, contact iaofflce@jpl.nasa.gov. NPO-47100

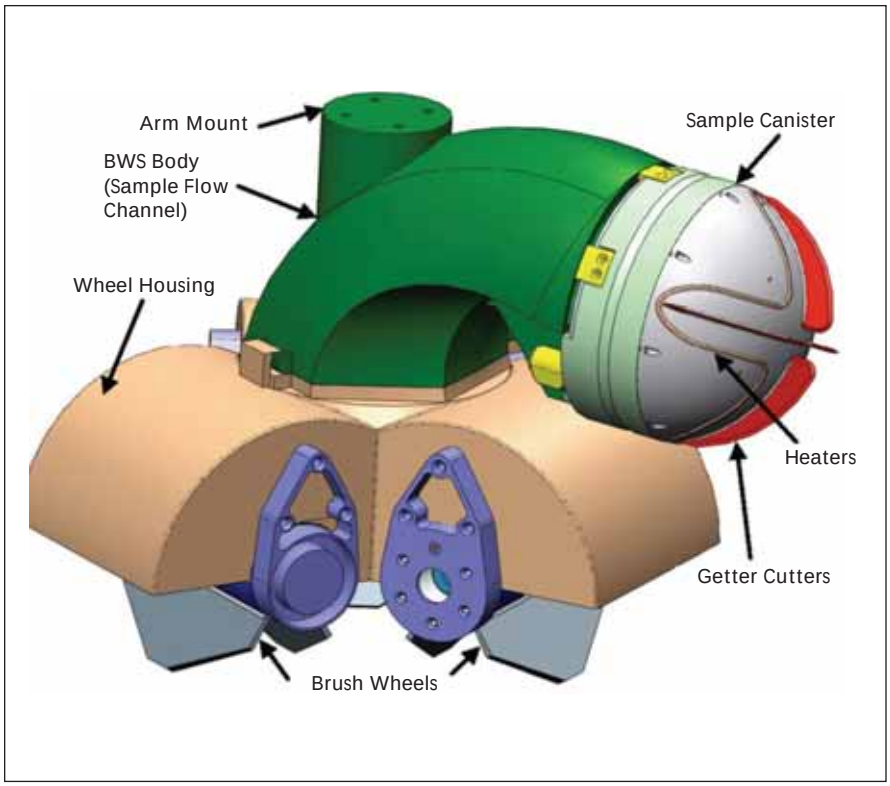

This **Brush Wheel Sampler,** similar to a common snow blower, is an effective sample collector.

Heterodyne Interferometer Angle Metrology

This technology can be used in optics, semiconductor, and other industries requiring high-precision angle metrology.

NASA's Jet Propulsion Laboratory, Pasadena, California

A compact, high-resolution angle measurement instrument has been developed that is based on a heterodyne interferometer. The common-path heterodyne interferometer metrology is used to measure displacements of a reflective target surface. In the interferometer setup, an optical mask is used to sample the measurement laser beam reflecting back from a target surface. Angular rotations, around two orthogonal axes in a plane perpendicular to the measurement-beam propagation direction, are determined simultaneously from the relative displacement measurement of the target surface. The device is used in a tracking telescope system where pitch and yaw measurements of a flat mirror were simultaneously performed with a sensitivity of 0.1 nrad, per second, and a measuring range of ±0.15 mrad at a working distance of an order of a meter. The nonlinearity of the device is also measured less than one percent over the measurement range.

Non-contact angular measurements are essential in numerous applications; for example, to monitor angle of mirror in telescopes used in astrometry, to control stages of x-ray interferometer, to measure Newton's constant using torsion balance, and to test equivalence principle using rotating masses. Two main methods used in angle measurements are traditional autocollimator technique and modern interferometry. Electronic autocollimators use a beam of collimated light on a flat external mirror reflecting the light back in the objective lens. The position of the spot in the focal plane of the lens is then correlated to the angular displacement of the mirror. Ultimate accuracy of the autocollimator is set by the diffraction limit.

A typical commercial autocollimator provides convenient angle measurement with sensitivity of ≈ 0.1 μrad with a few-centimeter-beam diameter. Another method is the use of Michelson interferometry, an interferometric method of measuring angle by counting change in interference fringe due to the variations of optical path difference (OPD) between reference plate and measurement plate under rotation. The interferometric technique suffers from nonlinearity in the OPD for the case of relatively large angle measurements. However, in small angle range, there are many variations of interferometer techniques developed based on internal reflection effects, fringe analysis, parallel interference pattern, and prism interferometer to achieve requirements for different applications.

In recent years, laser interferometers have been used widely in high-precision displacement measurements over length scales of nanometers to meters. The Michelson interferometry displacement sensor measures the phase of an optical wave as a measurement reflector is moved and infers the displacement in terms of λ, wavelength of the optical wave. Resolution of the displacement measurement is determined by noise on the optical signal and the instrument resolution of the phase detection. There are two main categories in the Michelson interferometer metrology. The homodyne interferometer (single frequency) using a quadrature detection is used in many applications where subnanometer resolution is not needed. For more accurate measurements with increasing resolution, heterodyne interferometry (two different laser frequencies) has been a widely used tool. One advantage of the heterodyne interferometer is that the phase information is carried on an AC signal rather than a DC signal. This makes it less sensitive to source laser power fluctuations, ambient light, and other slower noise affecting DC measurements. Also, a single detector is needed to measure both the displacement and the direction. By using acousto-optic modulators for heterodyne generation, many groups have achieved subnanometer level accuracy in the displacement measurements.

This work was done by Inseob Hahn, Mark A. Weilert, Xu Wang, and Renaud Goullioud of Caltech for NASA's Jet Propulsion Laboratory. For more information, contact iaoffice@jpl.nasa.gov. NPO-47179

Aligning Astronomical Telescopes via Identification of Stars

The alignment process would be completely automatic.

Marshall Space Flight Center, Alabama

A proposed method of automated, precise alignment of a ground-based astronomical telescope would eliminate the need for initial manual alignment. The method, based on automated identification of known stars and other celestial objects in the telescope field of view, would also eliminate the need for an initial estimate of the aiming direction. The method does not require any equipment other than a digital imaging device such as a charge-coupled-device digital imaging camera and control computers of the telescope and camera, all of which are standard components in professional astronomical telescope systems and in high-end amateur astronomical telescope systems. The method could be implemented in software running in the telescope or camera control computer or in an external computer communicating with the telescope pointing mount and camera control computers.

The image in the telescope field of view would be captured by the digital imaging device and digitized and then, according to the method, would be processed by a variant of any of several previously published star-identification algorithms. In simplified terms, such an algorithm determines criteria such as brightnesses and relative angles or distances between stars in the digital image and matches those criteria with stars in a database. Once such a match was found, the celestial coordinates of the identified objects in the image and the pixel coordinates of the object would be used to precisely determine the line of sight of the telescope in celestial coordinates.

Although the method does not require an initial estimate of the aiming direction, such an estimate (or ancillary information from which such an estimate can be calculated) could be used to accelerate the automated precise alignment process by limiting the search space to a small portion of the celestial-object database. Even if all that is known are the geographic coordinates of the telescope and the time, portions of the sky known not to be visible from that location at that time could be excluded from the search.

Once the celestial coordinates of two different lines of sight have been determined precisely as outlined above, the telescope would be automatically initialized and aligned for subsequent automated pointing and tracking. Thereafter, during tracking, the alignment process as described thus far could be repeated as often as desired to update the alignment: At each update, the celestial coordinates of the current line of sight would be communicated to the telescope control computer to maintain or restore the precise alignment of the telescope drive axes. Because the line-of-sight directions determined by this method would be based on direct observation of celestial objects having known coordinates, they would be more accurate than are the line-of-sight directions determined by prior methods that involve intermediate measurements (e.g., drive-shaft-angle measurements), which introduce drive-train and axis-misalignment errors.

This work was done by Mark Whorton of Marshall Space Flight Center.

This invention is owned by NASA, and a patent application has been filed. For further information, contact Sammy Nabors, MSFC Commercialization Assistance Lead, at sammy.a.nabors@nasa.gov. Refer to MFS-31968-1.

Generation of Optical Combs in a WGM Resonator From a Bichromatic Pump

A different approach to nonlinear oscillation excitation avoids undesired effects that previously limited optical comb quality.

NASA's Jet Propulsion Laboratory, Pasadena, California

Optical combs generated by a monolithic resonator with Kerr-medium can be used in a number of applications, including orbital clocks and frequency standards of extremely high accuracy, such as astronomy, molecular spectroscopy, and the like. The main difficulty of this approach is the relatively high pump power that has to be used in such devices, causing undesired thermorefractive effects, as well as stimulated Raman scattering, and limiting the optical comb quality and utility.

In order to overcome this problem, this innovation uses a different approach to excitation of the nonlinear oscillations in a Kerr-nonlinear whispering gallery mode (WGM) resonator and generation of the optical comb. By coupling to the resonator two optical pump frequencies instead of just one, the efficiency of the comb source can be increased considerably. It therefore can operate in a lower-power regime where the undesirable effects are not present. This process does not have a power threshold; therefore, the new optical component can easily be made strong enough to generate further components, making the optical comb spread in a cascade fashion. Additionally, the comb spacing can be made in an arbitrary number of the resonator free spectral ranges (FSR).

The experimental setup for this innovation used a fluorite resonator with

Ω = 13.56 GHz. This material has very low dispersion at the wavelength of 1.5 microns, so the resonator spectrum around this wavelength is highly equidistant. Light was coupled in and out of the resonator using two optical fibers polished at the optimal coupling angle. The gap between the resonator and the fibers, affecting the light coupling and the resonator loading, was controlled by piezo positioners. The light from the input fiber that did not go into the resonator reflected off of its rim, and was collected by a photodetector. This enabled observation and measurement of the (absorption) spectrum of the resonator.

The input fiber combined light from two lasers centered at around 1,560 nanometers. Both laser frequencies were simultaneously scanned around the selected WGMs of the same family. However, they were separated by one, two, three, or ten FSRs. This was achieved by fine-tuning each laser frequency offset until the selected resonances overlap on the oscilloscope screen. The resonator quality factor $Q = 7 \times 10^7$ was relatively low to increase the linewidth and, therefore, the duty cycle of both lasers simultaneously coupled into their WGMs. The optical spectrum analyzer (OSA) connected to the output fiber was continuously acquiring data, asynchronously with the laser scan. The instrument was set to retain the peak power values; therefore, a trace recorded for a sufficiently long period of time reflected the situation with both lasers maximally coupled to the WGMs.

This work was done by Dmitry V. Strekalov and Nan Yu of Caltech and Andrey B. Matsko of OEwaves for NASA's Jet Propulsion Laboratory. Further information is contained in a TSP (see page 1). **NPO-46253**

Large-Format AlGaN PIN Photodiode Arrays for UV Images

This UV detector can be used for measuring airborne particulates and for biological agent detection.

NASA's Goddard Space Flight Center, Greenbelt, Maryland

A large-format hybridized AlGaN photodiode array with an adjustable bandwidth features stray-light control, ultralow dark-current noise to reduce cooling requirements, and much higher radiation tolerance than previous technologies. This technology reduces the size, mass, power, and cost of future ultraviolet (UV) detection instruments by using lightweight, low-voltage AlGaN detectors in a hybrid detector/multiplexer configuration. The solar-blind feature eliminates the need for additional visible light rejection and reduces the sensitivity of the system to stray light that can contaminate observations.

The AlGaN UV detector operating at 325 nm gives a 1,000× better extraterrestrial solar radiation rejection than silicon. This reduced need for blocking filters increases the quantum efficiency (QE) and simplifies the optical systems. The wide direct bandgap reduces the thermally generated dark current to levels that allow many observations at room temperature. Because of this, the AlGaN UV photodiode array doesn't require the extensive cooling (and the associated cooling cost, complexity, and weight) that silicon does, significantly reducing system cost. Wide direct bandgap materials are naturally more radiation tolerant, which is crucial for instruments located outside of Earth's atmosphere.

The device is most sensitive to UV radiation when operated in the photovoltaic mode at or near zero-reverse bias voltage. The effect of the bandgap is seen at the long wavelength cutoff of 365 nm, and shows a contrast ratio before and after the cutoff edge of better than 10^3. Between 355 and 365 nm, the QE is fairly flat, with a high of 50 percent at 360 nm at –0.5 V bias. The QE falls rapidly with decreasing wavelength reaching a minimum of 3 percent at 345 nm. The detector's current responsivity at 360 nm and 0 V bias is 0.13 A/W. The spectral detectivity is 2.6×10^{15} cm $Hz^{1/2}W^{-1}$, corresponding to a detector noise equivalent power of 4.1×10^{-18} $W/Hz^{1/2}$.

While the benefits for space-based UV detection are readily apparent, there are Earth-based applications that can benefit as well. These include plume measurements, flame sensing, UV lidar, biological agent detection, and measuring airborne particulate size and velocity.

This work was done by Shahid Aslam and David Franz of Goddard Space Flight Center. Further information is contained in a TSP (see page 1). **GSC-15673-1**

Fiber-Coupled Planar Light-Wave Circuit for Seed Laser Control in High Spectral Resolution Lidar Systems

The compact, efficient, and reliable design enables use on small aircraft and satellites.

Langley Research Center, Hampton, Virginia

Precise laser remote sensing of aerosol extinction and backscatter in the atmosphere requires a high-power, pulsed, frequency doubled Nd:YAG laser that is wavelength-stabilized to a narrow absorption line such as found in iodine vapor. One method for precise wavelength control is to injection seed the Nd:YAG laser with a low-power CW laser that is stabilized by frequency converting a fraction of the beam to 532 nm, and to actively frequency-lock it to an iodine vapor absorption line. While the feasibility of this approach has been demonstrated using bulk optics in NASA Langley's Airborne High Spectral Resolution Lidar (HSRL) program, an ideal, lower cost solution is to develop an all-waveguide, frequency-locked seed laser in a compact, robust package that will withstand the temperature, shock, and vibration levels associated with airborne and space-based remote sensing platforms.

A key technology leading to this miniaturization is the integration of an efficient

waveguide frequency doubling element, and a low-voltage phase modulation element into a single, monolithic, planar light-wave circuit (PLC). The PLC concept advances NASA's future lidar systems due to its compact, efficient and reliable design, thus enabling use on small aircraft and satellites. The immediate application for this technology is targeted for NASA Langley's HRSL system for aerosol and cloud characterization. This Phase I effort proposes the development of a potassium titanyl phosphate (KTP) waveguide phase modulator for future integration into a PLC.

For this innovation, the proposed device is the integration of a waveguide-based frequency doubler and phase modulator in a single, fiber pigtail device that will be capable of efficient second harmonic generation of 1,064- nm light and subsequent phase modulation of the 532 nm light at 250 MHz, providing a properly spectrally formatted beam for HSRL's seed laser locking system. Fabrication of the integrated PLC chip for NASA Langley, planned for the Phase II effort, will require full integration and optimization of the waveguide components (SHG waveguide, splitters, and phase modulator) onto a single, monolithic device. The PLC will greatly reduce the size and weight, improve electrical-to-optical efficiency, and significantly reduce the cost of NASA Langley's current stabilized HSRL seed laser system built around a commercial off-the-shelf seed laser that is free-space coupled to a bulk doubler and bulk phase modulator.

This work was done by Anthony Cook of Langley Research Center and Shirley McNeil, Gregg Switzer, and Philip Battle of AdvR, Inc. Further information is contained in a TSP (see page 1). *LAR-17568-1*

On Calculating the Zero-Gravity Surface Figure of a Mirror

As well as gravity reversing between two configurations, mount forces must reverse to within the St. Venant scale.

NASA's Jet Propulsion Laboratory, Pasadena, California

An analysis of the classical method of calculating the zero-gravity surface figure of a mirror from surface-figure measurements in the presence of gravity has led to improved understanding of conditions under which the calculations are valid. In this method, one measures the surface figure in two or more gravity-reversed configurations, then calculates the zero-gravity surface figure as the average of the surface figures determined from these measurements. It is now understood that gravity reversal is not, by itself, sufficient to ensure validity of the calculations: It is also necessary to reverse mounting forces, for which purpose one must ensure that mounting-fixture/mirror contacts are located either at the same places or else sufficiently close to the same places in both gravity-reversed configurations. It is usually not practical to locate the contacts at the same places, raising the question of how close is sufficiently close. The criterion for sufficient closeness is embodied in the St. Venant principle, which, in the present context, translates to a requirement that the distance between corresponding gravity-reversed mounting positions be small in comparison to their distances to the optical surface of the mirror.

The necessity of reversing mount forces is apparent in the behavior of the equations familiar from finite element analysis (FEA) that govern deformation of the mirror. In FEA, the three-dimensional solid body (mirror) is approximated by a mesh of *N* points, and positions of these points, or nodes, are

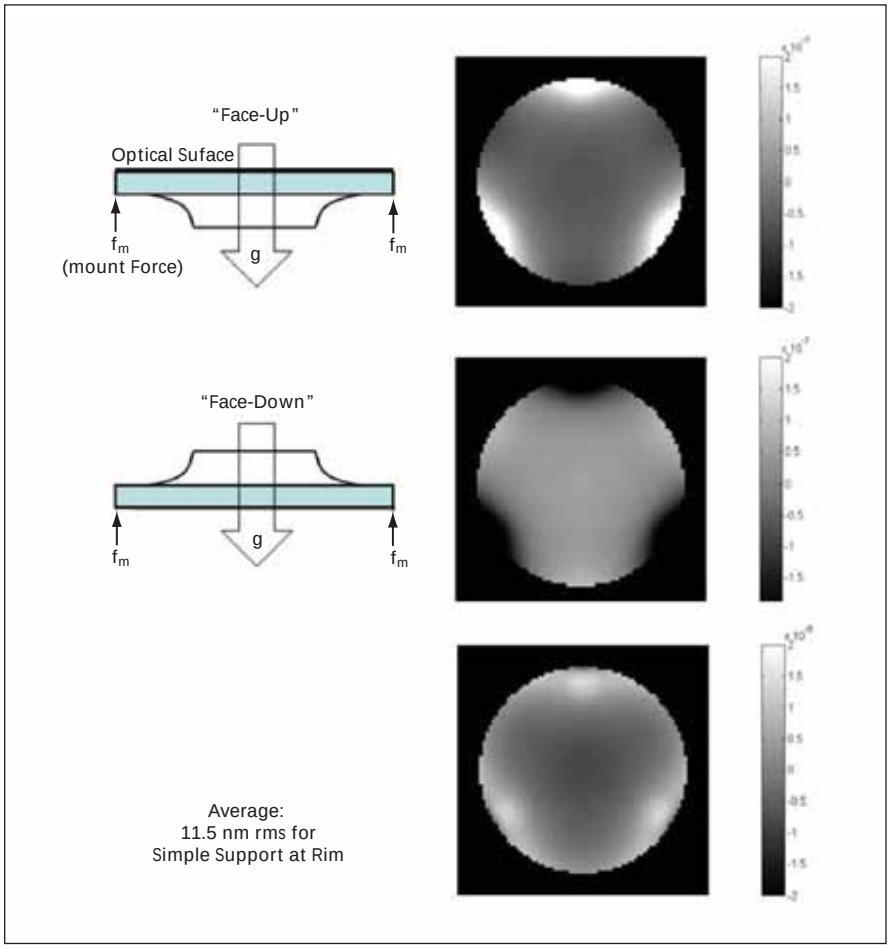

Fig. 1. **FEA Modeling of the Surface Figure** of PT-M1 during gravity reversal in a simple mirror mount in which the mirror rests on 3 points of contact near the rim (cartoons at left). The mirror model is specified to have a spherical surface in the absence of applied forces. The "face-up" and "face-down" orientations experience gravity forces that are reversed. However, mount forces in the two cases are applied at positions separated by the thickness of the mirror rim, so are only imperfectly reversed. Deformations in the two configurations are shown in the top two panels; their average is shown in the bottom panel, which recovers the ideal spherical surface (which would look flat in this display of departure from sphericity) marred by some dimple artifacts near the rim. The rms error in the average is 11.5 nm.

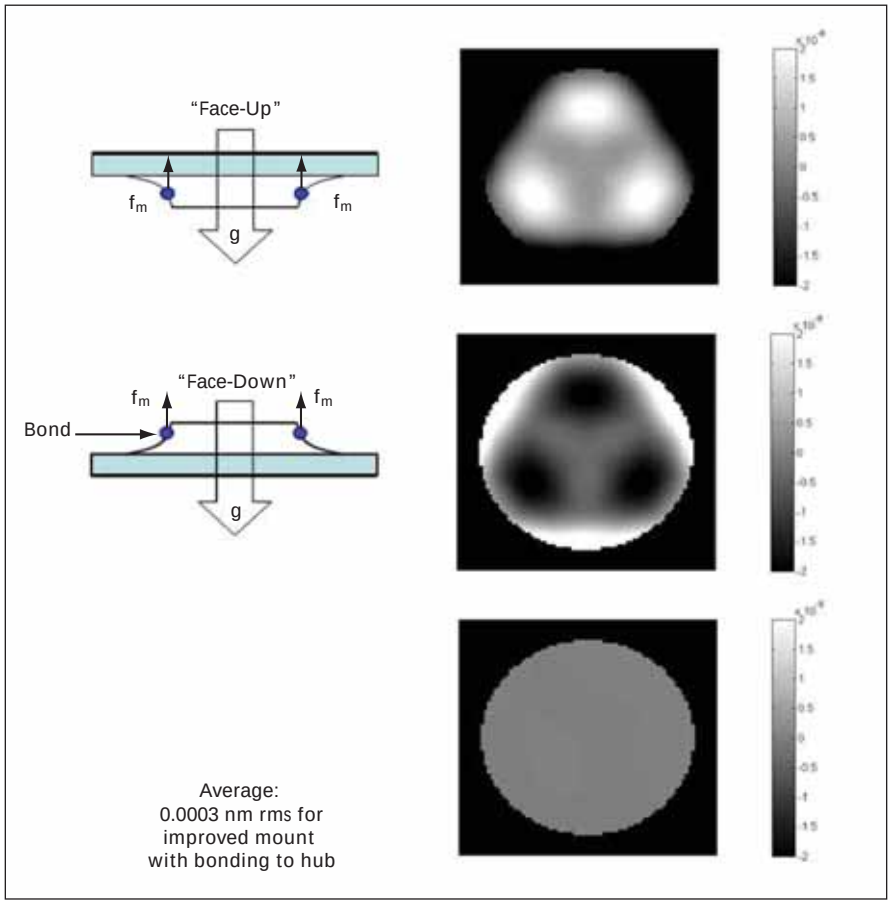

Fig. 2. **FEA Modeling of the Surface Figure** of PT-M1 during gravity reversal in an improved scheme incorporating good mount force reversal. The mount now consists of 3 point contacts bonded to the hub at the back of the mirror (cartoons at left); mount forces thus reverse and are applied at very nearly the same positions in the two orientations, far from the mirror surface. As a result, the surface figures (top two panels at right) are nearly exactly complementary, resulting in an average map (lower right panel) with a formal rms error of only 0.0003 nm.

represented by a 3*N*-dimensional coordinate vector $\mathbf{x}_i$. In the absence of forces, node positions are described by the zero-gravity position vector $\mathbf{x}_i^{0g}$ that we wish to extract. Forces, also represented by a 3*N*-dimensional vector $\mathbf{f}_i$, cause deviations $\delta\mathbf{x}_i$ from the zero-gravity mirror shape; the case of interest is normal gravity (1g), for which we may write the altered elemental positions as

$$\mathbf{x}_i^{1g} = \mathbf{x}_i^{0g} + \delta\mathbf{x}_i \quad (1)$$

These forces may be either body forces due to gravity ($\mathbf{f}^g$) or boundary forces due to the mirror mount ($\mathbf{f}^m$). The displacements may then be found from

$$A_{ij}\,\delta\mathbf{x}_j = f_i = f_i^g + f_i^m \quad (2)$$

where paired indices are summed over in the usual convention, and A_{ij} is the "stiffness matrix". The stiffness matrix is generally sparse, so that a given node is significantly affected only by a small number of nearby nodes; with suitable numbering, it will be nearly diagonal. In the mirror frame, the stiffness matrix does not change when the mirror is rotated among orientations. If the mirror is rotated into a new orientation in which body forces due to gravity reverse direction, and assuming that mount forces reverse as well, the new set of surface displacements $\delta\mathbf{x}_i'$ will obey

$$A_{ij}\cdot\delta\mathbf{x}_j' = f_i' = -f_i^g - f_i^m \quad (3)$$

in the frame of the mirror. Comparing to Equation (2) shows that

$$\delta\mathbf{x}_j' = -\delta\mathbf{x}_j \text{ for all j} \quad (4)$$

In other words, the average of the deviations from the ideal zero-gravity surface in the two orientations is zero, so the average figure is just the zero-gravity surface. Algebraically, this property may be expressed as

$$1/2(\mathbf{x}_i^{1g} + \mathbf{x}_i^{1g'}) = 1/2(\mathbf{x}_i^{0g} + \delta\mathbf{x}_i + \mathbf{x}_i^{0g} + \delta\mathbf{x}_i') = \mathbf{x}_i^{0g} \quad (5)$$

If forces do not reverse perfectly, localized surface artifacts or "dimples" will be seen on the zero-gravity mirror map. Precise gravity reversal is relatively easy to achieve, but some care must be taken to ensure that mount forces, f_i^m, also reverse. Furthermore, the reversed mount forces must be applied at the same points *i* of the mirror. The tolerance on placing mount forces in the two configurations is set by the St. Venant principle, which captures the basic annealing or space-averaging property of the elliptic partial differential equations governing solid-body deformations in the usual elastic, small-deformation regime. Remarkably, in practice, small position errors in force location are insignificant at distances through the glass of perhaps only 1.5 times their value.

A simple illustration of these principles is provided by the problem of mounting the PT-M1 mirror for zero-gravity surface figure testing. This mirror is a spherical prototype of the largest mirror of the SIM compressor in its former TMA (three-mirror anastigmat) design. The PT-M1 mirror measures about 343 mm in diameter, has a radius of curvature of about 2.2 m, and a surface quality spec of 6.3 nm rms ($\lambda/100$) under zero-gravity conditions. It has an areal density of 41.9 km-m^{-2}. This demanding surface spec, coupled with aggressive lightweighting, makes precise attention to mounting schemes critical during measurement of the zero-gravity surface if dimple artifacts are to be avoided. A rudimentary mounting scheme for "face-up/face-down" measurements whose average will yield the zero-gravity surface is shown in Figure 1. Support against gravity is provided from beneath the rim of the mirror, at two slightly different positions in the two configurations, and the result in the averaged surface map is dimpling at the position of the mounting points. The attendant measurement error (11.5 nm rms) exceeds the mirror spec.

A simple improvement to the mounting scheme is shown in Figure 2. Mount members are now attached by bonding, so mount forces in the two configurations are applied at identical positions. Also, mount members are attached to the hub of the mirror, well away from the mirror surface whose zero-gravity figure is being measured; by the St. Venant principle, small errors in effective positioning of mount members have little effect when propagated to the mirror surface. The resulting error in the zero-gravity averaged map is now only 0.0003 nm rms.

The principles described here represent an explicit clarification and deeper understanding of a classical technique for extracting the zero-gravity surface figure of a mirror from measurements of

multiple mounting configurations in normal gravity. While FEA computations are used to analyze particular candidate sets of mount configurations, these principles allow model-free insight into new configurations that are likely to be useful. Additional information and extensions of the particular mounting schemes presented here, including one that offers dramatically improved zero-gravity map fidelity without the need for bonding, are discussed in Bloemhof, Lam, Feria, and Chang, Appl. Opt. Vol. 46, No. 31, p. 7670 (2007).

This work was done by Eric E. Bloemhof of Caltech for NASA's Jet Propulsion Laboratory. For more information, contact iaoffice@jpl.nasa.gov.NPO-45685

Optical Modification of Casimir Forces for Improved Function of Micro- and Nano-Scale Devices

Manipulating these forces could result in improved MEMS devices.

NASA's Jet Propulsion Laboratory, Pasadena, CA

Recently, there has been a considerable effort to study the Casimir and van der Waals forces, enabled by the improved ability to measure small forces near surfaces. Because of the continuously growing role of micro- and nano-mechanical devices, the focus of this activity has shifted towards the ability to control these forces. Possible approaches to manipulating the Casimir force include development of composite materials, engineered nanostructures, mixed-phase materials, or active elements. So far, practical success has been limited. The role of geometrical factors in the Casimir force is significant. It is known, for example, that the Casimir force between two spherical shells enclosed one into the other is repulsive instead of normal attractive. Unfortunately, nanosurfaces with this topology are very difficult to make.

A more direct approach to manipulating and neutralizing the Casimir force is using external mechanical or electromagnetic forces. Unfortunately, the technological overhead of such an approach is quite large. Using electromagnetic compensation instead of mechanical will considerably reduce this overhead and at the same time provide the degree of control over the Casimir force that mechanical springs cannot provide. A mechanical analog behind Casimir forces is shown in the figure.

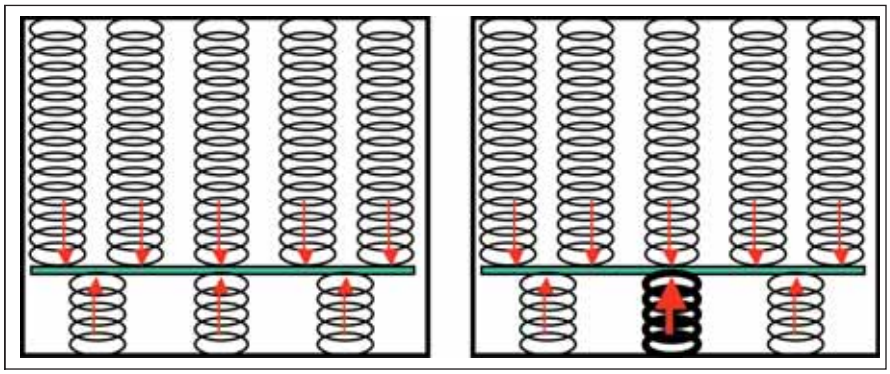

A **Mechanical Analog of the Casimir Force:** On the left, a net force arises from the difference in the number of compressed springs (the optical modes) attached to two sides of a partition. On the right, the Casimir force can be compensated, or even reversed, by making a certain spring "tougher" (i.e., eternally pumping the optical mode).

WGM (whispering gallery mode) resonators play an important role in modem optics and photonics because of their high quality factor and strong field localization. The optical field in such resonators is localized near the surface, resulting in a strong evanescent field. A new method takes advantage of the evanescent field of optical WGMs and utilizes them to control the Casimir force at a metal-dielectric interface. The main novelty of the approach lies in combination of state-of-the-art techniques for measuring the Casimir force with the optical WGM microresonators. The WGM resonators shaped as microspheres will be used. The evanescent field emerging from the microresonator surface will enable the desired capability of manipulating, neutralizing, and reversing the Casimir force.

In real MEMS (microelectromechanical system) applications, it may or may not be possible to utilize the optical evanescent field technique. The proposed approach relies on modification of the electromagnetic energy density in a vacuum gap, rather than on modification of material properties or of the microdevice shape. The advantage of this approach is that the new knowledge and techniques developed in its framework will be applicable to a much broader class of MEMS affected by Casimir force, in particular to those of practical importance. The optical evanescent field is just one example of various surface excitations that can modify the energy density in small gaps, therefore changing the Casimir forces. As another example, forces can be mediated by exciting surface plasmons instead of the evanescent field photons. Therefore, it will be possible to directly apply these theoretical results and experimental techniques to realistic metallic or silicon MEMS.

This work was done by Dmitry V. Strekalov and Nan Yu of Caltech for NASA's Jet Propulsion Laboratory. Further information is contained in a TSP (see page 1). ***NPO-46672***

Analysis, Simulation, and Verification of Knowledge-Based, Rule-Based, and Expert Systems

This method allows valid updates to be made quickly, efficiently, and without corruption of the existing rule base.

Goddard Space Flight Center, Greenbelt, Maryland

Mathematically sound techniques are used to view a knowledge-based system (KBS) as a set of processes executing in parallel and being enabled in response to specific rules being fired. The set of processes can be manipulated, examined, analyzed, and used in a simulation. The tool that embodies this technology may warn developers of errors in their rules, but may also highlight rules (or sets of rules) in the system that are underspecified (or overspecified) and need to be corrected for the KBS to operate as intended.

The rules embodied in a KBS specify the allowed situations, events, and/or results of the system they describe. In that sense, they provide a very abstract specification of a system. The system is implemented through the combination of the system specification together with an appropriate inference engine, independent of the algorithm used in that inference engine. Viewing the rule base as a major component of the specification, and choosing an appropriate specification notation to represent it, reveals how additional power can be derived from an approach to the knowledge-base system that involves analysis, simulation, and verification.

However, in a complex rule base that may have taken years, if not decades, to build, expecting users to have in-depth understanding of the rules that make up the system is not practical. This innovative approach requires no special knowledge of the rules, and allows a general approach where standardized analysis, verification, simulation, and model checking techniques can be applied to the KBS.

The rules of the system are likely written in a particular syntax, the possibilities for which include a language or grammar used by a particular inference engine, logic rules (written in Prolog or another logic programming or declarative programming language), propositional or predicate calculus, Horn clauses, or some form of structured English. A translator is required to translate these into the grammar of a tool that is used (and for which there is a prototype) to convert to a formal language that is process-based: that is, that recognizes that processes (or units of computation) are key components of a system.

All systems, regardless of how trivial, involve at least two processes, one being the environment in which the system is executing. Processes being enabled are analogous to rules firing; "deadlock" is equivalent to contradictions or internal inconsistencies existing in the rule base; "livelock" is equivalent to having rules that are unspecified; "top" is equivalent to overspecification; and "bottom" is equivalent to rules being underspecified. The system having been translated to the appropriate formal language, tools that already exist for that language may be applied to the analysis of the system. For example, if CSP were used as the formal language, the laws of CSP could be used to prove the absence, or otherwise, of contradictions, to pinpoint unimplemented rules, or to transform rules into a more efficient form. Then other available tools could be used for simulation and model checking.

This work was performed by Mike Hinchey, James Rash, John Erickson, and Denis Gracanin of Goddard Space Flight Center and Chris Rouff of SAIC. Further information is contained in a TSP (see page 1). **GSC-14942-1**

Core and Off-Core Processes in Systems Engineering

This methodology can reduce the difficulty of coordinating multiple systems-engineering activities.

NASA's Jet Propulsion Laboratory, Pasadena, California

An emerging methodology of organizing systems-engineering plans is based on a concept of core and off-core processes or activities. This concept has emerged as a result of recognition of a risk in the traditional representation of systems-engineering plans by a Vee model alone, according to which a large system is decomposed into levels of smaller subsystems, then integrated through levels of increasing scope until the full system is constructed. Actual systems-engineering activity is more complicated, raising the possibility that the staff will become confused in the absence of plans which explain the nature and ordering of work beyond the traditional Vee model.

Core activities are those that produce a top-down decomposition and bottoms-up integration of a system in order of increasing time. Examples of core activities are definition of requirements, design, acquisition, and integration. Because of ordering according to time, these activities are often readily understood and depicted by use of such elementary graphical aids such as timelines and Gantt charts.

Off-core activities are other systems-engineering activities that add desirable qualities to a system solution, but are not directly involved in decomposition and

integration. Examples of off-core activities are management of risk and opportunity, verification, validation, and troubleshooting. Because these activities are usually repeated many times and may not inherently be ordered in the same way as the core processes, they often cannot be represented by use of simple graphical aids. The complexity and difficulty of the task of representing off-core activities is increased by the fact that the timing and type of work involved in these activities are more unpredictable than are those of core activities.

In the present methodology, as applied to the development of a given system, the systems-engineering plan is organized to explicitly treat core and off-core activities separately. This approach to organization provides a conceptual framework that can facilitate and accelerate understanding, by members of the systems-engineering staff, of the relationships among many parallel activities. In so doing, this approach can reduce the difficulty of coordinating those activities.

This work was done by Julian C. Breidenthal of Caltech and Kevin Forsberg of the Center for Systems Management for NASA's Jet Propulsion Laboratory. For more information, contact Julian Breidenthal at julian.breidenthal@jpl.nasa.gov. NPO-45745

Digital Reconstruction Supporting Investigation of Mishaps

Lyndon B. Johnson Space Center, Houston, Texas

In support of investigations of mishaps like the crash of the space shuttle *Columbia*, a process based on digital reconstruction from recovered components has been developed. The process is expected to reduce the need for physical reconstruction from recovered parts, reduce the time and cost of determining the cause of a mishap, and provide information useful in redesigning to prevent future mishaps.

The process involves utilization of pre-existing techniques, hardware, and software to capture sizes and shapes of recovered parts in sets of digital data. The data are manipulated to enable rendering of captured geometric information by use of computer-aided design (CAD) and viewing software. The digitization of a part and study of its spatial relationship with other parts is taken to one of three levels of successively greater detail, depending on its importance to the investigation. The process includes a trajectory-analysis subprocess in which information from the digital reconstruction is combined with locations of recovered parts to reduce the area that must be searched to find other specified parts that have not yet been recovered. The digital product of the process is compatible with pre-existing CAD and solid-model-rendering software.

This work was done by William D. Macy and Robert B. Luecking of The Boeing Co. for Johnson Space Center. For further information, contact the JSC Innovation Partnerships Office at (281) 483-3809.

Title to this invention has been waived under the provisions of the National Aeronautics and Space Act {42 U.S.C. 2457(f)}, to The Boeing Co. Inquiries concerning licenses for its commercial development should be addressed to:

Terrance Mason,
Boeing Patent Licensing Professional
Mail Code 1650-7002
Boeing Management Co.
15460 Laguna Canyon Road
Irvine CA 92618
Phone No. (949) 790-1331
E-mail: terrance.mason@boeing.com
Reference: Boeing ID 03-0354

Refer to MSC-23783-1, volume and number of this NASA Tech Briefs *issue, and the page number.*

Template Matching Approach to Signal Prediction

An improvement is made in accurate prediction of future behavior and early detection of system problems.

NASA's Jet Propulsion Laboratory, Pasadena, California

A new approach to signal prediction and prognostic assessment of spacecraft health resolves an inherent difficulty in fusing sensor data with simulated data. This technique builds upon previous work that demonstrated the importance of physics-based transient models to accurate prediction of signal dynamics and system performance. While models can greatly improve predictive accuracy, they are difficult to apply in general because of variations in model type, accuracy, or intended purpose. However, virtually any flight project will have at least some modeling capability at its disposal, whether a full-blown simulation, partial physics models, dynamic look-up tables, a brassboard analogue system, or simple hand-driven calculation by a team of experts.

Many models can be used to develop a "predict," or an estimate of the next day's or next cycle's behavior, which is typically used for planning purposes. The fidelity of a predict varies from one project to another, depending on the complexity of the simulation (i.e. linearized or full differential equations) and the level of detail in anticipated system operation, but typically any predict cannot be adapted to changing conditions or adjusted spacecraft command execution. Applying a predict blindly, without adapting the predict to current conditions, produces mixed results at best, primarily due to mismatches between assumed execution of spacecraft activities and actual times of execution. This results in the predict becoming useless during periods of complicated behavior, exactly when the predict would be most valuable. Each spacecraft operation tends to show up as a transient in the data, and if the transients are misaligned, using the predict can actually harm forecasting performance.

To address this problem, the approach here expresses the predict in terms of a baseline function superposed with one or more transient functions. These transients serve as signal templates, which can be relocated in time and space against the

signal background. One then has the ability to reconstruct a signal regardless of the precise timing of the transients. During operation, one applies the actual start times of spacecraft activities as they occur, and produces a reconstructed, accurate predict in real-time.

This general approach is valid under two important conditions. First, the transients themselves must be time-invariant. Second, the transients must be reasonably consistent with respect to different operating points. Both of these assumptions are generally valid, but in the case of a complicated system with numerous types of overlapping transients, this approach may not be effective. Fortunately, there tend to be few transients in spacecraft telemetry of sensor quantities or low-level health and status information because these signals rarely reflect multiple different types of operation. Furthermore, if the predict is at least reasonably close to actual operation, the shift — either in time, or in the operating point when the transient occurs — is likely to be small.

The proposed approach considers three ways to recognize a transient. The first and most reliable is to use a different signal that identifies operating mode — often the transient will be correlated to a change in operating mode, and this change can usually be detected positively from discrete signals in spacecraft telemetry. If there is no useful mode signal, the second option is to identify the transient template by hand, and detect the onset of the transient using a curve-fitting approach. Finally, if one elects not to choose by hand, there is an option for automatic selection.

This technique has been applied to sensor data from several JPL missions and industrial applications, demonstrating an improvement in accurate prediction of future behavior and early detection of system problems. This technique is applicable to practically any time-varying, quantitative sensor measurement.

This work was done by Igor K. Kulikov and Ryan M. Mackey of Caltech for NASA's Jet Propulsion Laboratory. Further information is contained in a TSP (see page 1). ***NPO-47159***


NASA
National Aeronautics and
Space Administration